Geochemical and Sr-Nd isotopic study of Bay of Bengal sediments: Reconstruction of erosional changes during last Glacial-Interglacial cycle

A Thesis
submitted in partial fulfilment of the requirements for the BS-MS Dual Degree Programme

by

Priyasha Negi

20181091

Indian Institute of Science Education and Research

Pune 411008, India

April, 2023

under the guidance of

Dr. Gyana Ranjan Tripathy

Earth and Climate Science Department

IISER Pune

Certificate

This is to certify that this dissertation entitled **Geochemical and Sr-Nd isotopic study of Bay of Bengal sediments: Reconstruction of erosional changes during last Glacial-Interglacial cycle** towards the partial fulfilment of the BS-MS dual degree programme at the Indian Institute of Science Education and Research, Pune represents study/work carried out by **Priyasha Negi** at IISER Pune under the supervision of **Dr. Gyana Ranjan Tripathy**, Associate Professor, Department of Earth and Climate Sciences, during the academic year 2022-2023.

Priyasha Negi
(BS-MS Student)

Dr. Gyana Ranjan Tripathy
(Supervisor)

This thesis is dedicated to all my well wishers

Declaration

I hereby declare that the research work presented in the report entitled **Geochemical and Sr-Nd isotopic study of Bay of Bengal sediments: Reconstruction of erosional changes during last Glacial-Interglacial cycle** have been carried out by me at the Department of Earth and Climate Sciences, Indian Institute of Science Education and Research, Pune under the supervision of Dr. Gyana Ranjan Tripathy and the same has not been submitted elsewhere for any degree.

Priyasha Negi
(BS-MS Student)

Dr. Gyana Ranjan Tripathy
(Supervisor)

Acknowledgments

I would like to express my sincere gratitude to the following individuals and organizations who have supported me throughout my dissertation research at IISER Pune.

First and foremost, I would like to thank my supervisor, Dr. Gyana Ranjan Tripathy, for his guidance, support, and encouragement throughout my research work. His expertise and feedback have been invaluable in shaping my ideas and improving the quality of my work. I am grateful to my thesis expert, Dr. Devapriya Chattopadhyay for her feedback and constructive criticism during my mid-term evaluation which helped me to learn more things related to my research and strengthen my arguments.

I acknowledge LDEO core repository for providing us the core VM29-17 for this study. A part of the analyses for this thesis was conducted using XRF facility at IISER Pune, which was procured using financial support by the DST-FIST program. I am grateful to our collaborators Dr. Ravi Bhushan, PRL, India for the radiocarbon analyses and Dr. Santosh Rai and Dr. Satyabrata Das, WIHG, India for the Sr-Nd isotopic analyses.

This thesis could not have been successful without the constant support and guidance of my lab mate Rakesh Kumar Rout. I appreciate all the hard work and sincerity he put in towards teaching me and helping me with the analyses to finish this research project well ahead of time. I am deeply indebted to him and my other lab mates Achyuth Venugopal and Kruttika Mohapatra for their friendly demeanour and inclusive attitude which made me feel an integral part of the GRASP Lab. Their expertise and knowledge of the subject have helped me to refine my research and their dedication to scientific inquiry have been an inspiration to me.

Special thanks to Dr. Anupam Samanta, for his valuable contributions and willingness to lend a helping hand whenever needed. His insightful and critical feedback has been extremely helpful in shaping the final outcome of this project. I would also like to thank my parents, my sister, my friends and my ex-lab members Mohammad Amir and Ayrton for their unwavering support and encouragement throughout this journey. I want to thank you all as well as any overlooked individuals for your love and support that kept me grounded and motivated, even during the most challenging times.

Contents

List of Abbreviations

AMS – Accelerator Mass Spectrometry

AS – Arabian Sea

B/A - Bølling-Allerød

BCR – Basalt, Columbia River

BHVO – Basalt, Hawaiian Volcanic Observatory

BoB – Bay of Bengal

cmbsf – centimetres below sea floor

CIA – Chemical Index of Alteration

EICC – East Indian Coastal Current

ESL – Equivalent sea level

H1, H2, H3 – Heinrich event – 1,2,3

IBA – Indo-Burman Arakan

IDPs – Interplanetary Dust Particles

ISM – Indian Summer Monsoon

IWM – Indian Winter Monsoon

LDEO – Lamont-Doherty Earth Observatory

LGM – Last Glacial Maximum

MC ICP-MS – Multi-collector Inductively Coupled Plasma Mass Spectrometer

MIS – Marine Isotope Stage

MQ – Milli Q or deionised water

MWP – Melt water pulse

NE – North East

OIS – Oxygen Isotope Stage

PGG – Peninsular Granites and Gneisses

Q ICP-MS – Quadrupole Inductively Coupled Plasma Mass Spectrometer

REE – Rare Earth Elements

SW – South West

TTG – Tonalite Trondhjemite Granodiorite

WICC – West India Coastal Current

XRF – X-ray fluorescence

YD – Younger Dryas

List of Figures

List of Tables

Abstract

Chemical and isotopic signatures of oceanic sediments serve as a reliable tool to assess the interrelation between erosion and climate in the past. In this study, high-resolution geochemical and Sr-Nd isotopic data of a sediment core (VM 29-17PC; water-depth: 2813 m) from the western Bay of Bengal have been investigated. These data were used to reconstruct erosional and provenance changes in the Himalayas (relative to Indian Peninsula) during the last glacial-interglacial cycle. Radiocarbon dating of foraminifera from selected depths confirms that the 4.65-m long core archives an erosional record of the last 35 kyrs with no major hiatus. Geochemical trends, specifically increase in CIA and decrease in K/Al ratios, indicate an intensification in chemical weathering since 25 kyr. The $^{87}Sr/^{86}Sr$ (0.727 to 0.750) and $\varepsilon_{\mathrm{Nd}}$ (-18 to -14) values show significant temporal changes. These isotopic values, although intermediate to those reported for their major sediment sources, point to a dominant supply from Higher Himalayas (0.76, -15), and Deccan traps (0.705, -5) to the core-site. The isotopic trends with increasing $^{87}Sr/^{86}Sr$ and decreasing ε_{Nd} values between 15.3 to 5 kyr indicate an enhanced sediment contribution from the Himalayas during this period. This post-glacial increase in sediment supply from the Himalayas is synchronous to Bølling-Allerød (B/A) warm phase and a stronger Indian Summer Monsoon (ISM) phase, indicating a strong linkage between erosion and climate in kilo-year timescales.

1 Introduction

1.1 Introduction

Continental weathering and erosion play a crucial role in shaping Earth's landscape, climate and atmospheric composition over geological timescales. Weathering is the process by which rocks are broken down into smaller particles via physical, chemical, or biological forces whereas, erosion is the process of transporting weathered products from weathering site to the low-lying basins. Several geological (tectonics, basin slope and lithology), climatic (runoff, temperature, rainfall) and biological (vegetation) factors influence the weathering intensity in a river basin. Impact of these controlling factors, however, have been observed to vary significantly both at spatial and temporal scales. For example, in million years' timescale, carbonic acid-mediated weathering of silicate rocks is associated with CO_2 consumption from the atmosphere (Raymo and Ruddiman, 1992). These studies (Raymo and Ruddiman, 1992, Richter et al., 1992) have hypothesized that the late Cenozoic cooling (around 40 Myr ago) was a consequence of the tectonically driven increases in chemical weathering due to the upliftment of the Himalayan Tibetan Plateau. Recent studies have also focussed on how weathering can release CO_2 through organic carbon and sulfide oxidation, and cause global warming (Hilton and West 2020). The climate-erosion linkage becomes complicated over kilo years' time scale, as the exact role of these controlling factors and their strength to influence weathering and erosion patterns still remains to be completely understood (Tripathy et al., 2014; Samanta et al., 2022). The impact of climate on intensity, of both physical and chemical weathering processes, are found to differ in weathering or kinetically limited, and supply or transport limited regimes (West et al., 2005).

The Himalayas possess an exceptional physical erosion and chemical weathering pace (Milliman and Meade 1983), rendering them a captivating site to explore the temporal fluctuations in erosion patterns. The rivers flowing through the Himalayas deposit most of their sediments into the Bay of Bengal (Goodbred and Kuehl, 1999, 2000). Sediment contribution from the Himalayas is generally higher in the northern and western BoB due to high river runoff (Milliman and Syvitski, 1992). The Ganga and Brahmaputra rivers supply ~1060 million tons of sediments per year to the BoB, which is ~ 5% of the total riverine supply to the oceans from a discharge area of 1.59 million km^2 (viz. 1.3% of the total river discharge area in the world; Milliman and Syvitski, 1992). Other major rivers feeding the BoB annually are the Godavari (170 million tons), Krishna (64 million tons), Mahanadi, (60 million tons annually), and Irrawaddy (260 million tons). The Ganga-Brahmaputra River system mainly drain sediments from Higher Himalayas (HH) and Lesser Himalayas (LH) with HH dominating the contemporary supply (Singh et al., 2008). The Godavari and Krishna rivers bring sediments from both Deccan traps and the Peninsular granites and gneisses (PGG) while the Mahanadi only flows through PGG. The Irrawaddy brings sediments from the Indo-Burman Ranges and Arakan mountains (Tripathy et al., 2011 and references cited).

Available studies on temporal changes in Himalayan erosion in response to climatic changes have provided diverging views. Chemical and isotopic studies from the Ganga floodplain (Rahaman et al., 2009), and the western Bay of Bengal (Tripathy et al., 2014) have documented a decrease in the amount of sediment coming from Himalayas during the Last Glacial Maximum (LGM) due to limited areal exposure available for weathering over the Himalayas and weakening of SW monsoon during LGM. Similar studies from the Arabian sea (Cai et al., 2019) have also reported higher weathering rates observed in warm phase (high rainfall) compared to cool and dry phases (less rainfall) during the Holocene period, supporting the climate erosion linkage. In contrast, Sr-Nd isotopic studies of sediments from the central Bay of Bengal (Galy et al., 2009) and Arabian sea (Goswami et al., 2012) depict minimal change in erosion rates during climatic excursions. Further, von Blanckenburg et al. (2015) have directly measured relative weathering fluxes over glacial and interglacial periods, using Be isotope ($^{10}Be_{meteoric}/^{9}Be$) ratios to disagree the previously proposed "high rainfall-high weathering" hypothesis. Several other studies have also documented non-climatic factors to be the prime controlling parameters for erosion in millennial timescales (Bluth and Kump, 1994; Mandal et al., 2015; White et al., 1999). Although the exact cause for these differences is not known, the study area, basin sediment dispersal pattern, and the sediment sources' contributions can yield different results based on the climate sensitivity of erosion. The sediments of the BoB contain a comprehensive history of the changes in erosion intensity in the Himalayas, Peninsular India, and the Indo-Burman Ranges.

1.2. The Bay of Bengal: Geological and Oceanographic settings

The Bay of Bengal is situated in the north-eastern region of the Indian Ocean. It is bordered by the Indian Peninsula towards its north west and west, Bangladesh towards its north, and Myanmar and Andaman and Nicobar Islands towards its east as depicted in Fig. 1. Many large rivers such as Ganga, Brahmaputra, Godavari, Krishna, Mahanadi, Kaveri, Irrawaddy etc. flow into the BoB. The annual runoff reported into the BoB is 2,950 km^3 (Sengupta et al. 2006) which is more than 50% of freshwater influx in the entire tropical Indian Ocean. Due to this high freshwater influx, the surface waters of BoB have very low salinity (mean salinity reduces by about 7‰, Mohanty et al., 2008) on the other hand the AS (the north-western part of Indian Ocean) is highly saline due to excessive evaporation over this region. This Salinity difference within the Indian Ocean is somewhat equilibrated as the ocean circulates low salinity surface water from BoB to the AS via the EICC and WICC. This happens mostly during winters when the EICC flowing southward carries along with it the low saline waters from northern BoB and feeds it into the WICC flowing north into the AS. Apart from salinity gradient, the ocean water circulation is also influenced by monsoon winds, ocean currents and temperature (Vinayachandran et al., 2013).

The major sediment provenances of the western BoB are Himalayas and Peninsular India which mainly consists of Himalayas, Deccan traps and Archean terrains (PGG). The Himalayas are broadly classified into four sub-lithological units: (i) the Higher Himalayas (HH), (ii) the Lesser Himalayas (LH), (iii) the Tethyan Sedimentary Series (TSS), and (iv) the Sivaliks. The HH comprises granite, gneiss, migmatites and marbles. The LH consists of granite, gneiss weakly metamorphosed sedimentary rocks, metapelites and carbonates. The TSS primarily consists of sedimentary rocks that are weakly metamorphosed, along with carbonates and clastics, and the Sivaliks mostly contain quaternary alluvium, molasses and recycled Himalayan crust (Boral et al., 2021). Overall, the HH are major contributors of sediments to the western BoB (Singh et al 2008) due to the high river runoff and high elevation of these mountain ranges that facilitates erosion of sediments into the BoB. HH mostly has a granitic terrain which consists of highly radiogenic Sr ($^{87}Sr/^{86}Sr$ ratios 0.76) and less radiogenic Nd (ε_{Nd} values -15; Tripathy et al., 2011).

The Indian Peninsula is characterised by a wide array of lithology: (i) Archean cratons of Dharwar, Bastar, Singhbhum and Bundelkhand consisting of peninsular gneissic complex, granitic gneisses, phyllites, schists, amphibolites and tonalite-trondhjemite-granodiorite (TTG) (ii) Proterozoic mobile belts of Eastern Ghats, Aravalli, Satpura and Southern granulite terrain, consisting of khondalite, charnockite, leptynite etc.(iii) Palaeozoic and Mesozoic rocks of limestone, sandstone and conglomerates (of Gondwana) (iv) and the basaltic lava flows of Deccan Traps. These can be broadly narrowed down to two major provenances contributing sediments to the western BoB, the PGG and the Deccan basalts. The PGG comprises of granitic and gneissic terrain with $^{87}Sr/^{86}Sr$ of 0.737 and ε_{Nd} of -25 (data compilation from several studies, e.g. Goswami et al.,2012; Ahmad et al., 2009 etc.) and the Deccan basalts are enriched in radiogenic Nd (ε_{Nd} value of -5) but have lower radiogenic Sr ($^{87}Sr/^{86}Sr$ ratio equals 0.705) compared to Himalayas and PGG. These distinct Sr and Nd isotope values of the provenances are helpful in tracing any changes in the sediment contribution from different provenances with time. Sr and Nd isotopes are commonly used as indicators of sediment provenance. While both can provide valuable information about the source of sediments, Nd isotopes are generally considered more reliable proxy due to their higher resistance to fractionation during chemical weathering. Sr isotopes are also used to measure the effects of weathering and erosion, but when used in conjunction with Nd isotopes, they can provide a more robust characterization of sediment provenance.

The productivity of the BoB is relatively lower than that of Arabian Sea (AS) due to high freshwater influx and stratification, preventing the upwelling of deep nutrient rich layers to the photic zone, where photosynthesis can occur (Prasanna Kumar et al.,2002). Verma et al. (2022) have reported that the BoB's productivity has varied over time, with high productivity during the last glacial period (weak ISM) and low productivity during the following deglacial and Holocene periods (strong ISM). During the subsequent deglacial and Holocene periods, the SW monsoon (ISM) was relatively strong and predominantly responsible for providing freshwater influx to the BoB, thereby reducing productivity due to the increased stratification that hindered nutrient upwelling to the photic zone. However, during the glacial periods, the ISM was relatively weaker leading to reduced stratification and increased mixing in the water column. The strong NE monsoon winds during this time further strengthened the vertical advection of the nutrient rich deeper layers to the photic zone. The reversal of these seasonal winds can also directly affect the circulation of BoB. Hydrographic study by Babu et al., 2003 and other contemporaries reveal seasonality in water circulation: anticyclonic (anticlockwise) circulation is dominant during the NE monsoon and collapses as the SW monsoon intensifies. With the intensification of SW monsoon, cyclonic (clockwise) circulation dominates the bay till winter monsoon starts again.

1.3 Objective of the thesis

The main objectives of the thesis are:

- To present high-resolution geochemical and Sr-Nd isotopic analyses of a sediment core from the western Bay of Bengal.
- Reconstruction of the erosional history of the Himalayas in the last glacial-interglacial cycle and their linkage to the climate changes, if any, during the last 35 kyrs.

Temporal changes in these chemical and isotopic data for the VM29-17 core, together with available data for their major sedimentary sources, are expected to provide better insights on the climatic sensitivity of the Himalayan erosion in kilo-year timescale. This will also provide a mechanistic view of climate-erosion coupling in millennial timescale.

1.3 Structure of the thesis

The overall structure of this thesis can be divided into four main sections:

- **Section 1** – briefly explains the weathering and erosion processes and their relationship with climate in geological timescales. It also summarises some of the contemporary studies and describes the geological and oceanographic setting of the study area (Bay of Bengal).
- **Section 2** – provides a detailed analytical protocol that has been followed for various geochemical and isotopic analyses (such as radiocarbon dating, inorganic carbon, major oxides, trace elements and Sr-Nd isotopic measurements) in this study.
- **Section 3** – presents the outcomes of the analyses described in section 2. It is divided into two main sub-sections (i) Results – where all the outcomes from the analyses (described in section 2) are stated and (ii) Discussion – where we try to comprehend and interpret the results.
- **Section 4** – summarizes all the work that has been accomplished, the major findings, and their corresponding interpretations.

2 Material and Methods

2.1 Core Description

We have used the sediment core VM29-17PC from the western Bay of Bengal (Lat - 16°38'N and Long - 85°24'E; Fig. 1) for this study. It was retrieved by R/V Vema cruise in the year 1971 from a water depth of 2,813 m and archived at Lamont-Doherty Earth Observatory (LDEO) Core Repository, New York. The core is 465 cm long and is mostly composed of clay. It is moderately olive grey in colour, moist, firm and lightly

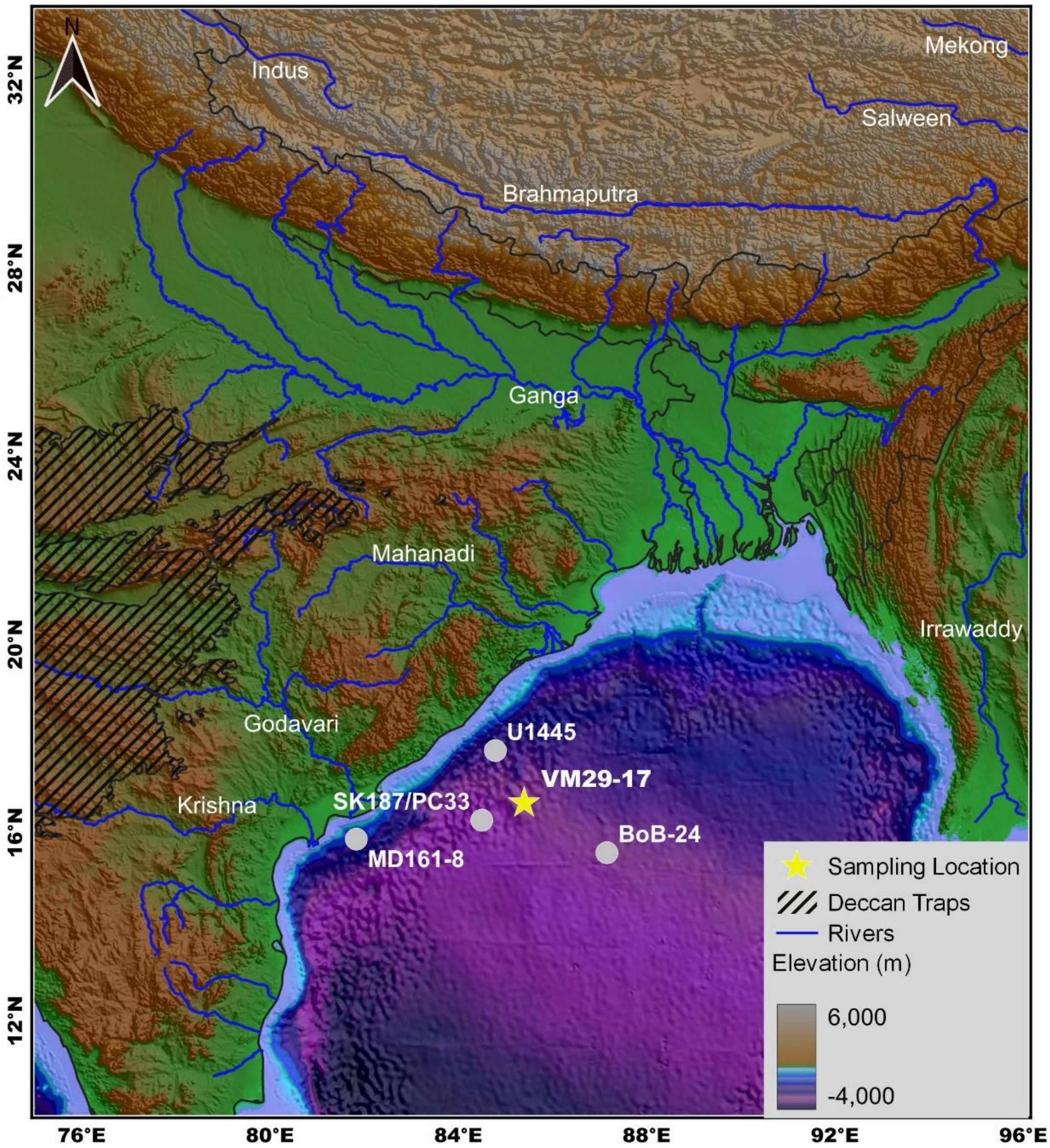

Fig. 1 *Location map of the VM29-17PC core. Earlier-studied cores from near-by locations [SK187/PC33 (Tripathy et al., 2014), MD161-8 (Peketi et al., 2020), U1445 (Lee et al., 2022), and BoB-24 (Liu et al., 2021)] are also shown.*

burrowed. Coarse fractions are negligible and it consists quartz, planktic foraminifera, Radiolaria, echinoid spines and manganese micronodules. A small layer of coarse fraction is present at a depth 111-113 cmbsf mainly consisting of - sub-angular to rounded quartz, common to rare planktic foraminifera, benthic foraminifera, pteropods, occasional igneous rock fragments, pyrite aggregates and negligible corals. This core was subsampled at 1 cm interval for every 5 cm depth at LDEO, and a total of 88 samples were shipped to IISER Pune for geochemical analyses.

.

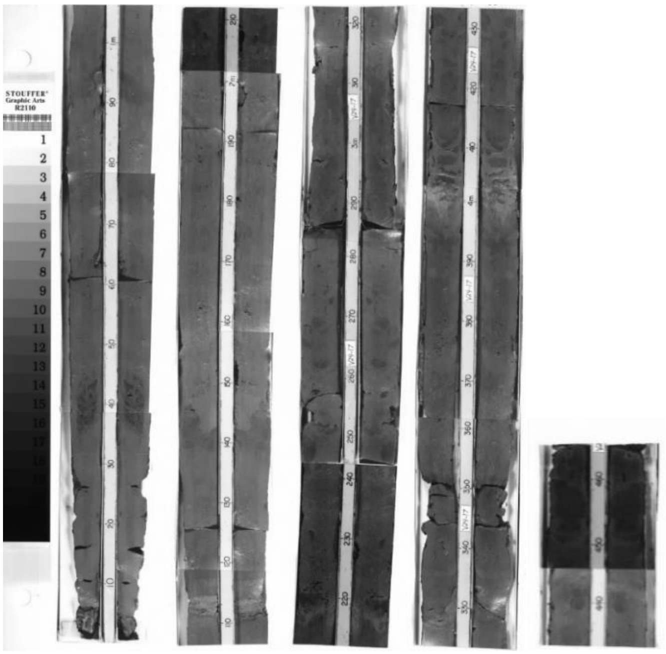

Fig. 2 *Picture of the VM29-17 sediment core. (Picture source: NOAA)*

Fig. 3 *Sample picture of mixed planktic foraminifera ((a) Globigerina bulloides, (b) Globorotalia menardii) for the sediment (from depth 190-191 cmbsf) picked for ^{14}C dating.*

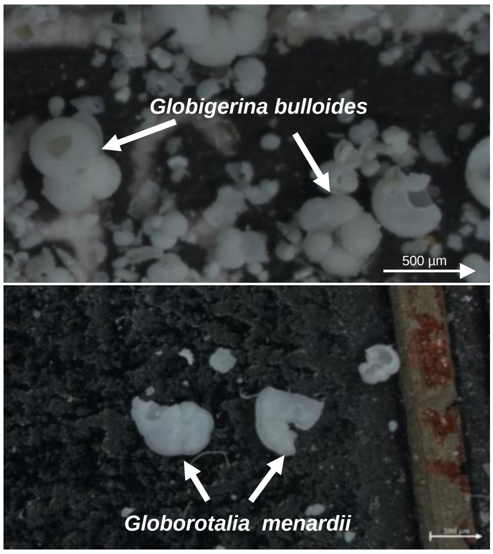

2.2 Radiocarbon dating

To establish the chronology of the core, mixed planktic foraminifera (such as *Globigerina bulloides, Globorotalia menardii* etc.) from 11 selected depths were subjected to radiocarbon analysis using the AMS (Accelerator Mass Spectrometry) facility at Physical Research Laboratory, India (Table 1). Towards this, ~5g of sample from each depth was dried in an oven overnight at 60°C, and washed with MQ. The water-washed samples were treated with Sodium Hexametaphosphate to decoagulate the clay particles. Subsequently, the sediments were treated with H_2O_2 to remove all the organic matter from the sample. From this aliquot, the clay was separated from the

Table 1 AMS ^{14}C ages of the VM29-17 piston core sediments.

S. No.	Lab ID	Depth (cm)	Radiocarbon Age Years	Calibrated Age Range	Median Age Years
1	17PC-06	25-27	1089 ± 36	601-764	679
2	17PC-15	75-76	3340 ± 35	3161-3358	3256
3	17PC-21	110-111	8499 ± 37	9056-9276	9169
4	17PC-29	150-151	5787 ± 60	6095-6315	6206
5	17PC-36	190-191	10272 ± 38	11360-11646	11511
6	17PC-40	210-211	11717 ± 43	13132-13318	13232
7	17PC-44	230-231	14835 ± 46	17197-17513	17364
8	17PC-52	270-271	18327 ± 56	21349-21643	21513
9	17PC-57	300-301	20855 ± 66	24137-24455	24294
10	17PC-63	335-336	16013 ± 79	18594-18846	18712
11	17PC-72	380-381	26293 ± 101	29763-30013	29881

sand fraction using a sieve (230 µm) and the foraminifera present in the sand fraction were picked out under the reflected light microscope in Paleobiology lab at IISER Pune after it was dried. These foraminifera were analysed for their radiocarbon ages using the AMS facility at PRL. The measured ^{14}C dates were calibrated using Calib 8.2 (Stuiver and Reimer, 1993) and corrected for reservoir age of ΔR = -195 ± 51 (Dutta and Bhushan, 2001). We notice two outliers (age reversals) at a depth 110 - 111 cm and another at depth 335 - 336 cm. These age reversals could be a result of several factors such as sediment disturbance, bioturbation, contamination during experiment, etc. It is worth mentioning here that the samples from the depth 110-111 cmbsf are close to a sand-horizon, unlike other sediments which are mostly clayish in nature. Hence, we discard these two dates to assign the ages of the remaining depth via linear interpolation and extrapolation (Fig. 4).

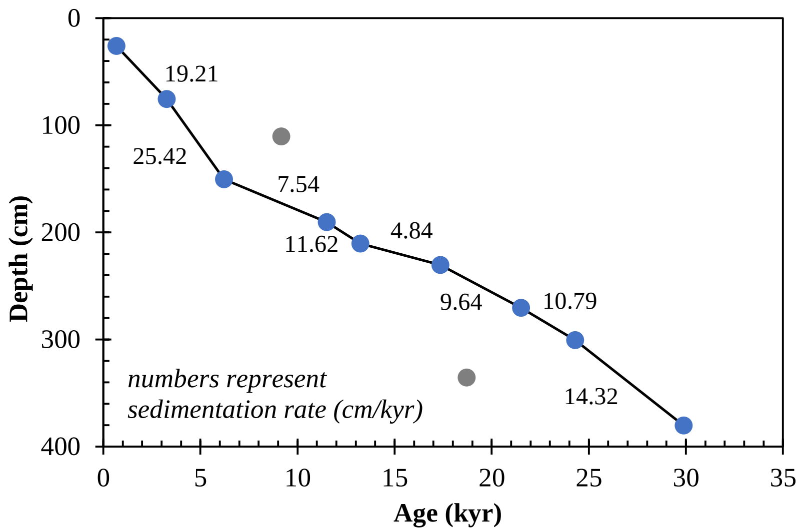

***Fig. 4** Depth-age relationship for the VM29-17 core using radiocarbon ages of foraminifera samples. Two outliers (shown in grey circles) are not included in constraining the chronology.*

The sedimentation rates vary from 4.84 to 36.82 cm/kyr, with an average of 16.19 cm/kyr. The average time resolution of our geochemical analyses for VM29-17 core is 77 years (ranging from 27 to 207 years).

2.3 Geochemical and Isotopic Analyses

Geochemical and Isotopic analyses of the sediment core were carried out using the same methodology as outlined by Tripathy et al., 2011 and 2014. Around 5g of sample was taken and dried in an oven at 60°C overnight. After drying, these samples were powdered using agate mortar and pestle, and sieved to ~100µm size. The powdered samples were washed thoroughly using deionized water to remove sea salts. These water-washed sediments were then dried and powdered. The powdered aliquots of the water-washed sediments were used for $CaCO_3$ measurement, whereas decarbonated fractions of these sediments were used for other geochemical and isotopic analyses.

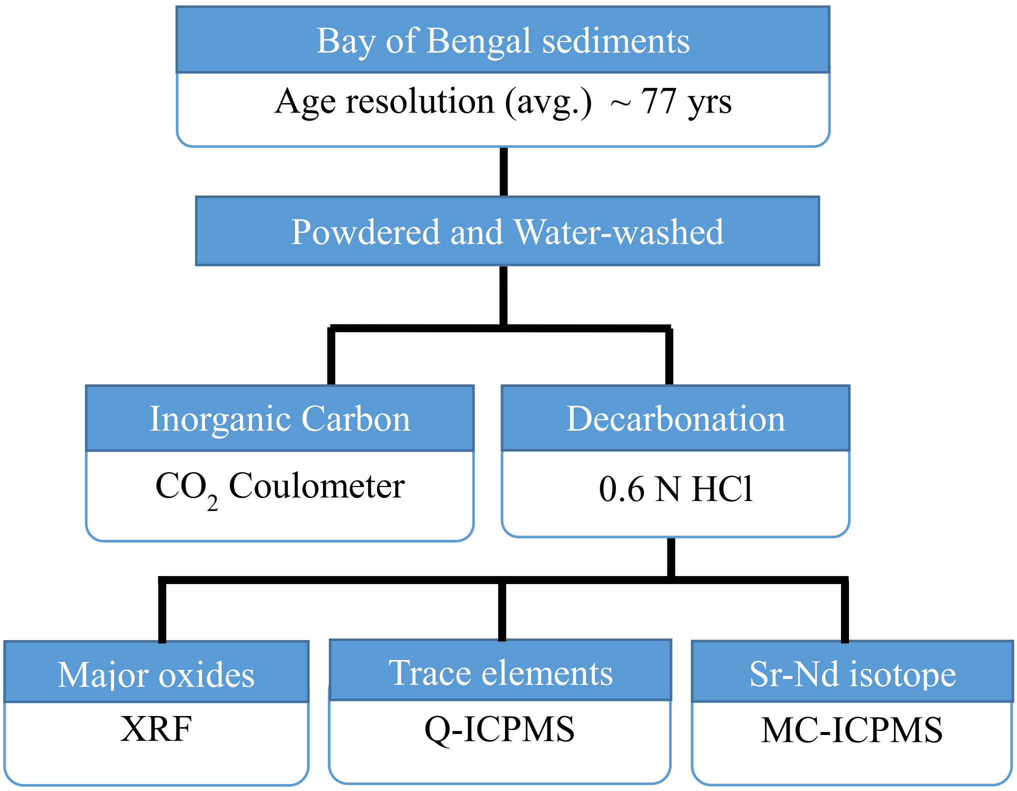

Fig. 5 *Flowchart of the chemical and isotopic analytical methodology adopted during this study.*

2.3.1 Inorganic Carbon ($CaCO_3$)

The samples were analysed for their carbonate content, which was measured using a CO_2-coulometer. For this, ~15mg of the powdered sample was treated with ortho-phosphoric acid at a temperature of 80°C to release CO_2 gas from the carbonate phases, both calcite and dolomite. The amount of CO_2 released are quantified in the Coulometer to measure the concentration of carbonates ($CaCO_3$) present in the samples. The accuracy and precision of the data are always better than ± 6%.

2.3.2 LOI and Major Oxides

Concentrations of the major oxides are measured in the decarbonated fraction of the sediments. To remove carbonates from the sample, approximately 2g of powdered sample was treated with 0.6 N HCl at 80°C temperature. These decarbonated samples were used to measure the major oxides using X-Ray Fluorescence (XRF) analyzer. For XRF analysis, the samples were fused with a flux at 1100°C in a platinum crucible to prepare a fusion bead. This bead preparation requires 1/17 ratio of sample/flux (set for the XRF calibration method). Around 0.55g of sample, ~9.35g of flux (lithium metaborate/lithium tetraborate) and a few drops of releasing solution (anhydrous lithium bromide) have been used. We have ashed the decarbonated samples at 550°C to constrain the loss on ignition (LOI). The Bruker XRF analyzer measures the major oxides concentrations using Geoquant Advance standard calibration method with an accuracy and precision of ±2 % and ±1% respectively. We have used the major oxides data to compute the chemical index of alteration (CIA), which serves as a good proxy for degree of chemical weathering in the river basins. The sediments' CIA values were determined using the equation (Eqn. 1) provided by Nesbitt and Young, 1982.

$$\text{CIA} = \frac{\mathrm{Al_2O_3}}{\mathrm{Al_2O_3 + Na_2O + K_2O + CaO^*}} \times 100 \qquad (1)$$

In this equation, the abundance of oxides is expressed in molar units, and CaO* refers to the concentration of CaO in the silicate fraction of the sediment. Apart from CIA, a modified index, CIA*, has also been employed as a measure of weathering. The CIA* is calculated using equation 2 (Tripathy et al., 2014):

$$\text{CIA*} = \frac{\mathrm{Al_2O_3}}{\mathrm{Al_2O_3 + Na_2O + K_2O}} \times 100 \qquad (2)$$

2.3.3 Trace elements and Sr-Nd Isotopes

The decarbonated and ashed samples were used to measure the trace element concentrations, and Strontium and Neodymium isotopic ratios. To achieve this, roughly 0.1g of samples were digested using combination of HF-HNO_3-HCl acids in the Anton Paar Microwave Digestion System. After microwave digestion, the residues left, if any, is further treated with several cycles of Aqua Regia (3:1 ratio of HCl: HNO_3) to dissolve the samples thoroughly. These dissolved solutions (in 0.32 N HNO3 medium) were analysed for their trace elemental concentrations using a Q ICP-MS (Thermo-scientific iCAP) instrument at IISER Pune. To ensure the accuracy of the data, two certified geochemical reference materials (USGS BCR-2 and BHVO-2) were utilized, and the precision was confirmed by conducting multiple measurements, both of these were always within ±10%.

Sr-Nd isotopic measurements were carried out for twenty-five samples. These analyses were carried out using MC-ICPMS facility at WIHG, Dehradun on commercial basis. For this, dissolved solutions of the decarbonated samples were passed through a cation exchange resins (Bio-Rad AG50W-X8 (200-400µm)) to extract the pure fractions of Sr and REEs. The REEs fraction collected was again passed through a Eichrom LNspec^{TM} (50-100) resins (Pin et al., 2014) to extract pure Nd. Isotopic ratios $^{87}Sr/^{86}Sr$ and $^{143}Nd/^{144}Nd$ were measured using a Neptune plus thermo-scientific MC ICP-MS at WIHG. To ensure high quality measurements international standards NBS-987 (for Sr) and JNdi-1 (for Nd) were used. The average $^{87}Sr/^{86}Sr$ value of the NBS-987 standard was 0.71029 ± 0.00001 (n = 6), whereas the average $^{143}Nd/^{144}Nd$ for the JNdi standard was 0.512088 ± 0.000003 (n = 10). These values match well with its reported values (Singh et al., 2008, Borghini et al., 2016). The Nd isotopic data is expressed in terms of epsilon (ε) notation as:

$$\varepsilon_{Nd} = \left[\frac{^{143}Nd/^{144}Nd_{Sample}}{^{143}Nd/^{144}Nd_{CHUR}} - 1\right] \times 10^4 \qquad (3)$$

Here $^{143}Nd/^{144}Nd_{Sample}$ is the measured Nd isotopic ratio for our sediment and $^{143}Nd/^{144}Nd_{CHUR}$ is 0.512638 (Jacobsen and Wasserburg, 1984) which is the present-day $^{143}Nd/^{144}Nd$ value of Chondritic Uniform Reservoir (CHUR). Two procedural blanks were also run along with samples; the average blank values for Sr (~2200pg) and for Nd (~600pg) were found negligible compared to the total amount of Sr and Nd processed.

3 Results and Discussion

3.1 Results

The inorganic carbonate content, which can be supplied by both detrital and biogenic sources, varies significantly throughout the core. We have calculated the calcium carbonate ($CaCO_3$) concentrations from the inorganic carbon measured via CO_2 Coulometer which basically represents the carbonate content (both calcitic and dolomitic) in the samples. Carbonate content of the samples vary between 1.38 and 24.4 wt% with mean value of 8.34 ± 5.72 wt%, (n = 88), which is comparable to that reported for a nearby core SK187/PC33 (~7 wt%; Tripathy et al., 2014). Based on the carbonate concentration variations, we can divide the depth profile into three intervals, 35.5 to 25.3 kyr, 25.3 to 12.8 kyr, and 12.8 kyr to present (Fig. 6). The carbonate content is highest during the time interval of 12.8 to 25.3 kyr (avg. 15.18 wt%) which coincides with the glacial period. These concentrations are relatively low in the other two intervals with least values observed for the Holocene sediments (avg. 5.88 wt%).

Table 2 Average major and trace elemental compositions of the VM29-17 core are compared with those reported for the major sedimentary sources (Data source: Tripathy et al., 2014; Bastia et al., 2019)

		Ganga	Brahmaputra	Godavari-Krishna	Mahanadi	VM29-17
Na		0.7	1.3	0.6	0.7	0.6
Mg		1.5	1.6	1.5	0.2	1.0
Al		7.9	8.0	8.0	5.2	8.8
K	**wt%**	2.3	2.6	1.7	3.8	2.3
Ca		2.1	1.4	2.0	0.8	0.3
Ti		0.5	0.4	0.8	0.2	0.6
Fe		4.6	4.1	6.4	2.7	4.1
CIA*		77	71	81	60	79
Ba		448	510	205	1089	173
V		100	93	192	53	117
Cr		95	102	129	100	65
Cu		40	32	91	35	43
Ni	**µg/g**	47	49	84	25	52
Zn		90	86	151	30	104
Sr		88	136	140	114	54
Co		15	16	30	14	13
Mn		908	1000	800	-	338

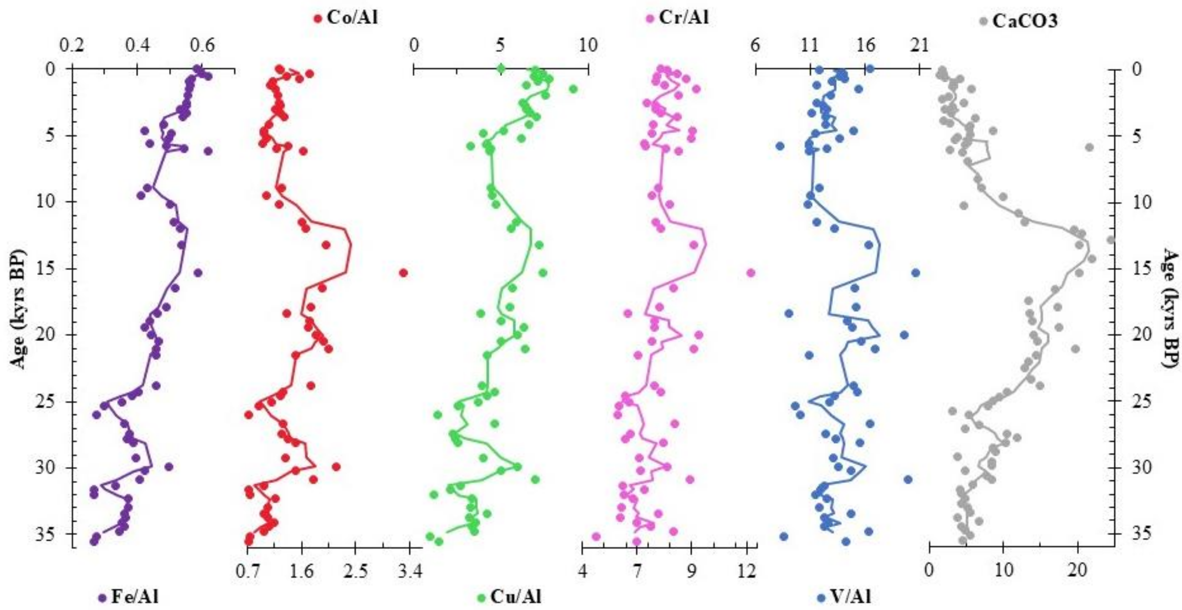

Fig. 6 *Down-core variations in carbonate content and Al-normalised ratios of selected elements (Fe, Co, Cu, Cr and V) for the VM29-17 core.*

Concentration of Na (0.26 – 1.38, avg. 0.61 ± 0.25 wt%), Mg (0.73 – 1.29, avg. 1.0 ± 0.1 wt%), Al (7.27 – 9.44, avg. 8.84 ± 0.37 wt%), K (1.66 – 2.91, avg. 2.33 ± 0.28 wt%), Ti (0.42 – 0.63, avg. 0.56 ± 0.03 wt%), Fe (2.11 – 5.49, avg. 4.07 ± 0.85 wt%), Si (24.07 - 31.46, avg. 26.31 ± 1.34 wt%) P (0.01 - 0.02, avg. 0.01 ± 0.003 wt%) show significant depth variation. Table 2 compares the average concentrations for these elements from VM29-17 core with their possible major sedimentary sources, viz. Ganga-Brahmaputra (Garzanti et al.,2011), Godavari-Krishna (Pattan et al., 2008), and Mahanadi Rivers (Bastia et al., 2019). Most of these values fall within the endmember compositions, except for Al and Ca. The observed difference for Al and Ca could be due to measurement of these data in different phases (bulk for sediment sources versus decarbonated for VM29-17 samples) in these studies. The computed CIA and CIA* values vary between 64 and 84 (avg. 77 ± 5, n=88), and 70 and 85 (avg. 79 ± 4, n=88), respectively. The CIA values show a monotonous increase since last ~26 kyr from 69.78 to 83.59 (Fig. 7). A simultaneous decrease is also observed in K/Al ratio with small fluctuations around ~5 kyr. Further, the chemical indices for provenances, such as Fe/Al and Ti/Al ratios, also show increasing trends between 26.18 kyr to 13.59 kyr and late Holocene period implying an increase in sediment contribution from Deccan during these time periods.

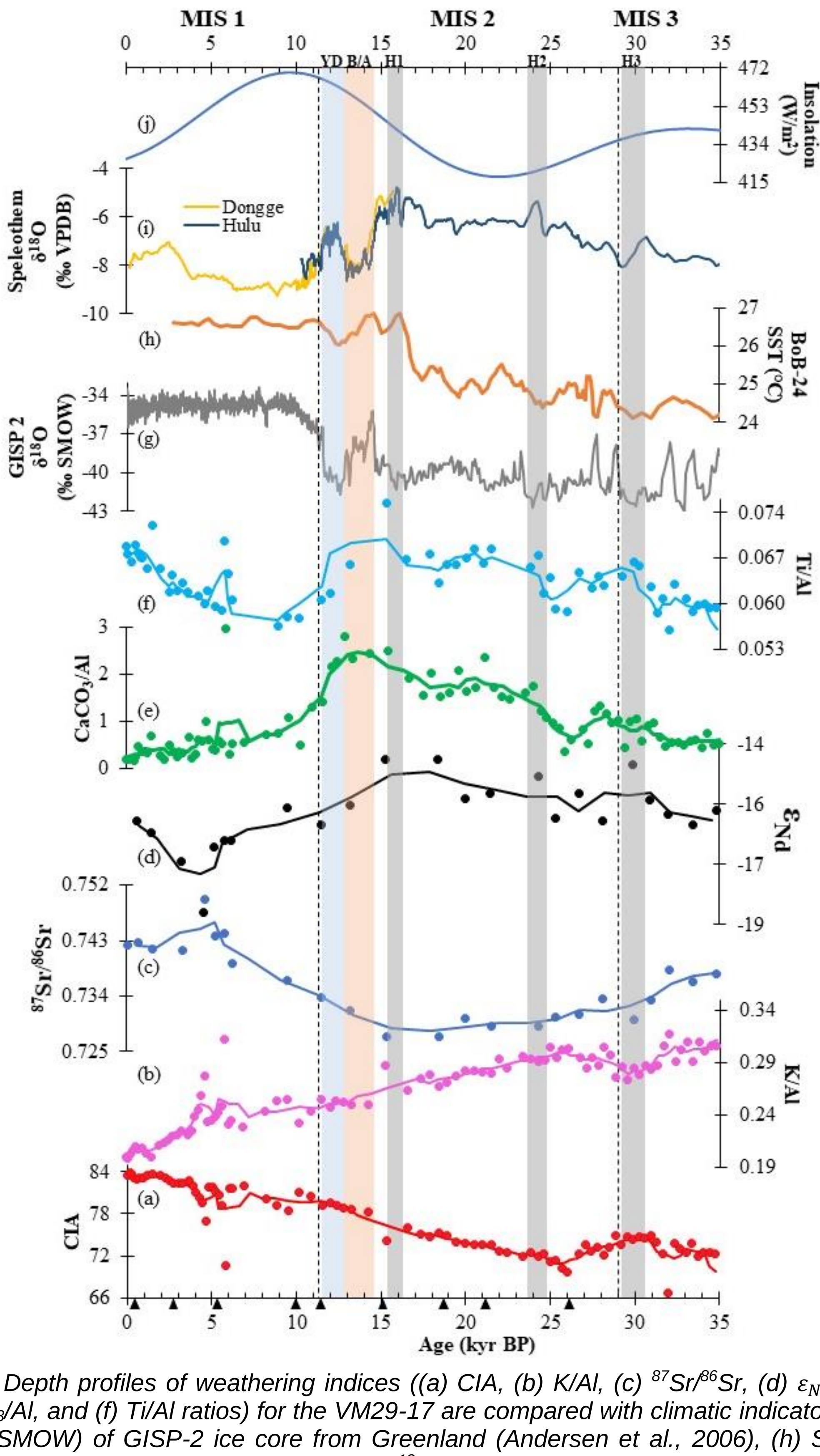

Fig. 7 *Depth profiles of weathering indices ((a) CIA, (b) K/Al, (c) $^{87}Sr/^{86}Sr$, (d) ε_{Nd}, (e) $CaCO_3/Al$, and (f) Ti/Al ratios) for the VM29-17 are compared with climatic indicators ((g) $\delta^{18}O$ (SMOW) of GISP-2 ice core from Greenland (Andersen et al., 2006), (h) SST of nearby core BoB-24 (Liu et al., 2021), (i) $\delta^{18}O$ (VPDB) of speleothem from Dongge and Hulu caves (Wang et al., 2001; Yuan et al., 2004) and (j) Solar insolation (Berger et al., 1991). The black triangles stand for the ^{14}C AMS dates.*

Table 3 Correlation matrix of the major and trace elemental data of the VM29-17 sediments.

	Na	K	Ca	Mg	Al	Fe	Ti	C_{inorg}	Ba	Cr	Mn	Sr	V	Co	Cu	Ni	Zn
Na	1.00																
K	0.87	1.00															
Ca	0.99	0.82	1.00														
Mg	-0.12	-0.06	-0.09	1.00													
Al	-0.46	-0.14	-0.52	0.12	1.00												
Fe	-0.93	-0.89	-0.89	0.34	0.35	1.00											
Ti	-0.67	-0.58	-0.64	0.48	0.37	0.73	1.00										
C_{inorg}	0.24	0.21	0.29	0.50	-0.50	-0.12	-0.01	1.00									
Ba	0.09	-0.01	0.14	0.25	-0.31	0.09	0.07	0.25	1.00								
Cr	-0.65	-0.50	-0.64	0.33	0.26	0.65	0.56	0.05	0.20	1.00							
Mn	-0.21	-0.27	-0.18	0.31	0.01	0.37	0.41	0.08	0.34	0.25	1.00						
Sr	0.40	0.28	0.44	0.25	-0.48	-0.22	-0.07	0.44	0.83	-0.14	0.21	1.00					
V	-0.12	-0.01	-0.14	0.42	0.10	0.17	0.46	0.18	0.19	0.67	0.36	0.08	1.00				
Co	-0.25	-0.24	-0.21	0.69	-0.21	0.44	0.49	0.59	0.54	0.54	0.44	0.49	0.55	1.00			
Cu	-0.82	-0.79	-0.80	0.32	0.24	0.83	0.70	-0.04	0.06	0.75	0.19	-0.19	0.41	0.49	1.00		
Ni	-0.75	-0.68	-0.71	0.56	0.20	0.83	0.69	0.23	0.26	0.85	0.37	-0.02	0.53	0.74	0.84	1.00	
Zn	0.04	0.03	0.06	0.11	-0.11	0.03	0.16	0.08	0.11	-0.02	0.09	0.14	0.06	0.25	0.10	0.08	1.00

Consistent to major elemental trends, concentrations of trace element in VM29-17 core also show notable temporal variations. The concentrations of V (60-175 µg/g), Cr (36-95 µg/g), Mn (119-1938 µg/g), Co (6-27 µg/g), Ni (20-89 µg/g), Cu (7-77 µg/g), Zn (8-423 µg/g), Sr (16-170 µg/g), and Ba (10-1020 µg/g) show variations of different magnitude, with highest variation being observed for Ba and lowest for Cr. Concentrations of most of the trace elements fall within the range of values reported for Ganga, Brahmaputra, Godavari-Krishna and Mahanadi except for Cr, Co, Mn, Sr and Ba which are relatively lower. We observe difference in concentrations of these elements due to measurement of source and core sediments in different phases.

Selected major and trace element concentrations, despite of large temporal variability, exhibit good correlation with each other (Table 3). The C_{inorg} concentrations only show positive correlation with Sr (0.44) and Co (0.59). The Fe concentration (immobile element; mostly supplied by continental sources) although show positive correlation with Ti (0.73), Cu (0.83) Ni (0.83) and Cr (0.65), it has a significant negative correlation with Na (-0.93), K (-0.89), and Ca (-0.89). These three mobile elements (Na, K and Ca) show strong correlation (> 0.82) with each other, and are also strongly negatively correlated to Cu (< -0.79). Further, strong correlations between three transition elements (Cu, Ni and Cr; >0.75) point to similar sediment sources for elements. The alkali earth metals, Sr and Ba, show a positive correlation, hinting at similar provenance of these elements to the core site.

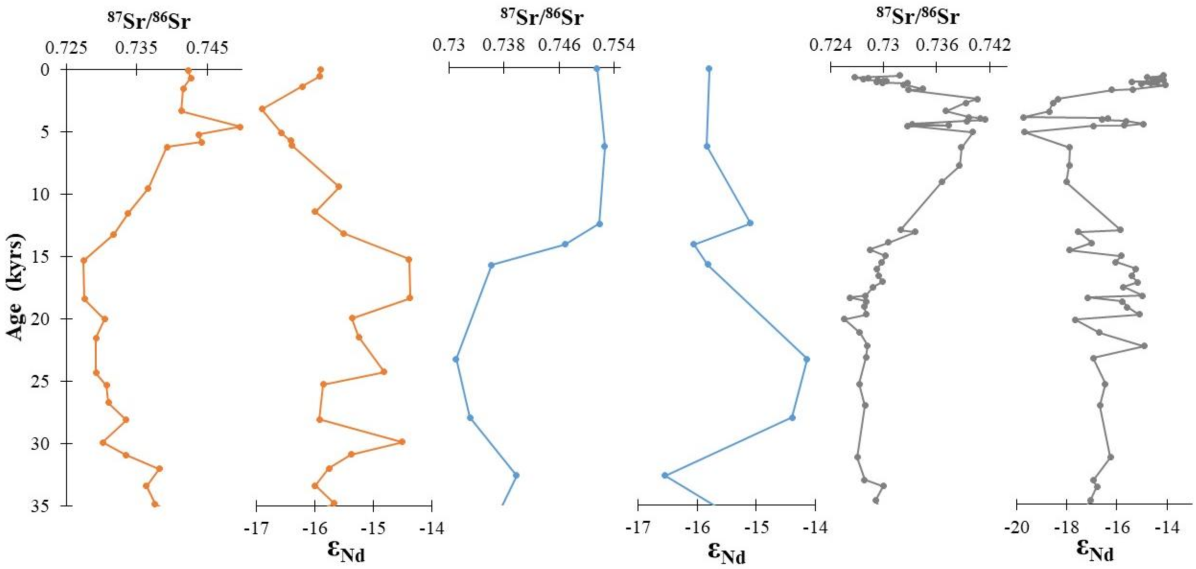

Fig. 8 *Temporal variations in $^{87}Sr/^{86}Sr$ and ε_{Nd} ratios for the (a) VM29-17 core. For reference, these isotopic trends for near-by cores ((b) U1445 (Lee et al., 2022), and (c) MD161-8 (Peketi et al., 2020)) are also shown.*

The $^{87}Sr/^{86}Sr$ and ε_{Nd} concentrations in the silicate fraction of the VM29-17 sediments also shows significant down-core variations ((0.72742 to 0.74969, avg. 0.7360 ± 0.594, 1σ, n = 25) and (-18.20 to -14.37, avg. -15.76 ± 0.81, 1σ, n = 25) respectively) during the last glacial and interglacial period (Fig. 7 and Fig. 8). These isotopic values for the sediments are intermediate to those reported for their possible sediment provenances (Singh et al., 2008; Tripathy et al., 2011), viz. HH (0.76, -15), LH (0.85, -24.4), Deccan (0.705, -5), and PGG (0.737, -25). Further, our Sr-Nd isotope data are found comparable with the previously reported data from near-by cores in the western BoB. For instance, Sr-Nd isotope values in silicate fraction of sediment core UI445 ranges from 0.731 to 0.753 for $^{87}Sr/^{86}Sr$ and -18.6 to -14.1 for ε_{Nd} (Lee et al., 2022) and core SK187/PC33 isotope values ranges from 0.72528 to 0.75732 for $^{87}Sr/^{86}Sr$ and -21.1 to –13.7 for ε_{Nd} (Tripathy et al., 2011). Another core MD161-8 also shows Sr-Nd isotope variations within the range of 0.72477 to 0.74155 for $^{87}Sr/^{86}Sr$ and -19.72 to -14.05 for ε_{Nd}. The temporal changes in the Sr and Nd isotopic data for VM29-17, U1445, MD161-8 are shown in Fig. 8. These trends for VM29-17 show anti-correlation between Sr and Nd isotopic trends, with systematically lower $^{87}Sr/^{86}Sr$ values and higher ε_{Nd} values (avg. 0.729, -14.8 resp.) being observed between the depth intervals of 220 and 301 cmbsf. These depths correspond to a sediment deposition time interval of 15.3 -24.3 kyrs BP. Subsequently, the Sr isotopic values depict steady increase from 0.727 to 0.750 between 15.3 to 5 kyr. Synchronously, the ε_{Nd} values also show decline decrease simultaneously from -14.4 to -18.2. These isotopic changes point to significant (relative) change in sediment supply from the major sources to the core-site during last 35 kyr.

3.2 Discussion

Marine sediments are mainly composed of detrital, biogenic, authigenic, hydrothermal (from hydrothermal vents) and cosmogenic (from extraterrestrial cosmic dust) components. Out of these, cosmogenic and hydrothermal sources' contribution may not be significant in basins with high freshwater influxes. As mentioned earlier, the BoB receives high sediment fluxes from the Himalayan and Peninsular Indian rivers and hence, these sediments are dominantly supplied by terrigenous sources. However, inorganic carbon contents in oceanic sediments can be supplied by both detrital and biogenic/authigenic sources. The carbonate ($CaCO_3$) content shows significant fluctuation during the deposition of these core sediments (Fig. 6 and Fig. 7). The relatively higher concentrations are observed during the MIS-2 (cold period) as compared to the MIS-1 and MIS-3 (warm periods). This could be possibly linked to the decrease in sea level during that time (Lambeck et al., 2014) and related weathering of carbonate phases in the exposed shelf sediments.

3.2.1 Chemical Weathering patterns during last 35 kyrs

As discussed earlier marine sediments are a mixture of detrital, biogenic and authigenic components, however, to reconstruct past erosion patterns and provenance changes we require only the detrital component of the sediments. Towards this, Al-normalized ratios of mobile or immobile elements have found frequent applications (Tripathy et al., 2014). Al is an immobile major element that mainly comes from continental or terrestrial sources, hence normalizing with Al corrects for the authigenic factor and gives the detrital contribution of elements. During chemical weathering, loss of mobile elements such as K is observed from the bedrock. As chemical weathering increases the bedrock is depleted in mobile elements, however, concentration of immobile elements (that are resistant to weathering) such as Al is not affected by this process. Thus, an increase in chemical weathering will result in a decrease in K/Al ratio and vice versa. Another weathering proxy proposed by Nesbitt and Young (1989) is the Chemical Index of Alteration (CIA) which is basically a ratio of immobile to mobile elements (Eqn. 1; Section 2.3.2). A modified version CIA* (Eqn. 2; Section 2.3.2) works similar to CIA and has been computed and compared with the major sources (Table 2). The CIA* values are higher for more weathered rocks as compared to the unweathered bed rock and keeps increasing as the intensity of weathering increases. For e.g. the HH and LH have CIA* values of 65 and 58 respectively, however the sediments of the rivers draining these lithologies viz. Ganga and Brahmaputra have relatively higher CIA* values (77 and 71 resp.; France Lanord and Derry, 1997; Singh et al., 2008) due to alteration of source rocks. Similarly, the Godavari-Krishna river sediments also have higher CIA* values (81; Das and Krishnaswami, 2007) as compared to the major source rock viz. Deccan (78; Mahoney et al., 2000).

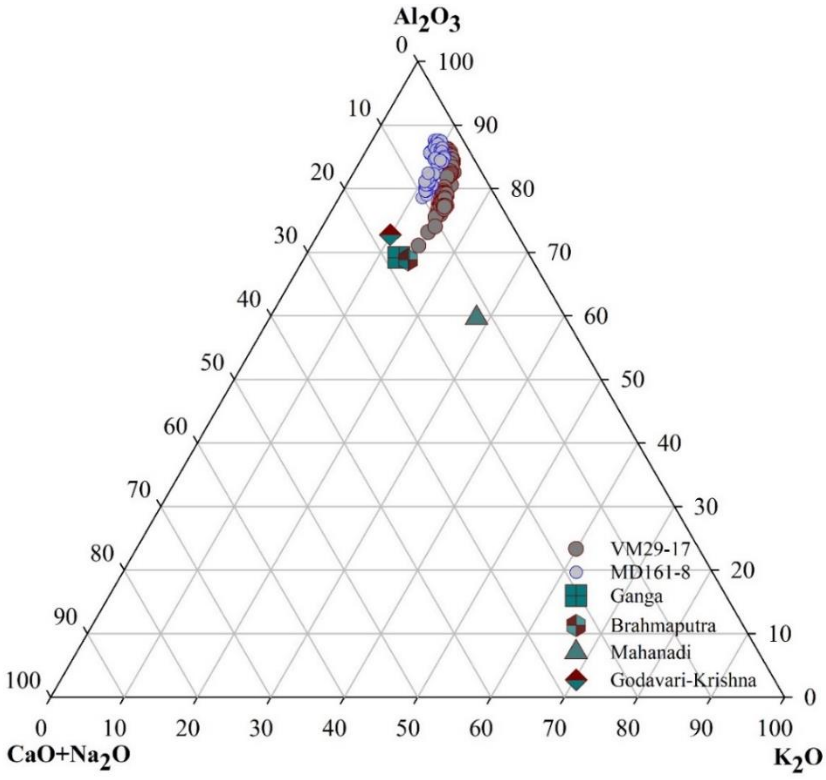

Fig. 9 *A-CN-K (Al_2O_3-CaO+Na_2O-K_2O) ternary plot. Data for nearby core (MD161-8; Peketi et al.,2020) and their major riverine sources are also plotted.*

The CIA* values for the VM29-17 core has been constantly increasing since last ~26 kyr with an average values of 79 ± 4 (n=88) which lies intermediate to those reported for its sources primarily the Deccan and Himalayan rivers. An extension to CIA is the A-CN-K (Al_2O_3-CaO+Na_2O-K_2O) ternary plot which shows similar results (Fig. 8). Basically as weathering intensifies there is more and more loss of K_2O, Na_2O and CaO due to which the composition shifts towards the Al_2O_3 apex. A simultaneous decrease in K/Al ratio is also observed around the same time indicating an intensification in chemical weathering. These changes can also be influenced by size sorting, however, after correction for size sorting also we observe similar trend which implies that there has been an increase in chemical weathering. Another factor that can influence the CIA and K/Al trends is the changes in the sediment provenance. The CIA* and K/Al values for HH and Deccan are different (65 and 0.36 for HH; 78 and 0.06 for Deccan) so any change in the provenance is equally capable of changing these values. To solve this problem, we measure the Sr-Nd isotopes to trace the provenance changes during the last 35 kyrs.

3.2.2 Sediment provenance changes

The Sr-Nd isotope values of the major sources are distinct (0.76 $^{87}Sr/^{86}Sr$ and -15 ε_{Nd} for HH; 0.705 $^{87}Sr/^{86}Sr$ and -5 ε_{Nd} for Deccan) which makes it possible to use these as provenance indicators. In addition, Nd is a reliable provenance indicator as the rare earth element is very resistant to chemical weathering and does not fractionate from sediment during weathering processes. This geochemical property of Nd prevents any influence of chemical weathering in the Nd isotope data. The $^{87}Sr/^{86}Sr$ and ε_{Nd} values of the VM29-17 core vary from 0.727 to 0.750 (avg. 0.736 ± 0.006, n=25) and -18.2 to -14.4 (avg., -15.8 ± 0.8, n=25) respectively. These values fall within the mixing lines joining Deccan, HH and PGG (Fig. 10) which suggests that the sediment supply is majorly from these three sediment provenances. The sample points are closer to the Deccan and HH mixing line, with closest proximity to HH signifying its dominant contribution at all times.

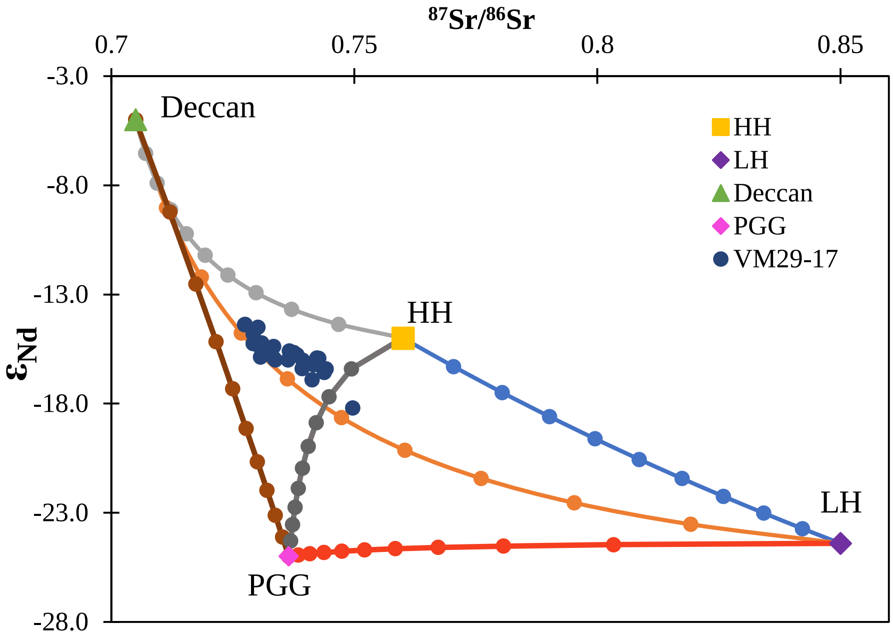

Fig. 10 *Source mixing trends between $^{87}Sr/^{86}Sr$ and ε_{Nd} of the VM29-17 core.*

Temporal variation in Sr-Nd isotope show no significant changes until 15 kyr, after which a simultaneous decrease in Sr isotope and increase in Nd isotope indicates high sediment supply from Himalayas. Previous studies (Tripathy et al., 2014) have documented higher sediment supply from Deccan during LGM and increase in Himalayan contribution immediately after the LGM. However, the high chronology data from this study observes relatively stable provenance contribution during the time interval of 35 kyr to 15 kyr. The increase in sediment supply from Himalayas around 15 kyr is synchronous to the B/A warm phase after which sediment contribution from the Deccan increases again around 5 kyr till present. A similar Sr-Nd isotope trend is also observed by Peketi et al. (2020) for a core (MD161-8) located near the Godavari-Krishna basin (Fig. 8). The isotopic values for MD161-8 ranges from 0.725 to 0.742 (avg. 0.732 ± 0.005, n=53) for Sr and -19.7 to -14.1 (avg. -16.2 ± 1.4, n=53) for Nd in the last 35 kyr (Peketi et al., 2020).

The increase in chemical weathering observed around 26 kyr, therefore, is independent of the provenance changes, as there were no significant provenance changes till 15 kyr according to the Sr-Nd data. After 15 kyr, the sediment supplies from Himalayas increased and since CIA* values of Himalayas are lesser than that of Deccan, we would expect lower CIA* values, however this is not the case, rather the CIA* keeps increasing at this time as well. Hence, we can say that the weathering proxies calculated are not substantially influenced by provenance changes and that there are significant changes in chemical weathering for the studied period. A similar increase in CIA is also observed for nearby cores (Lupker et al., 2013; Peketi et al., 2020).

3.2.3 Comparison with paleoclimate proxies

Fig.7 compiles some of the different proxies used in this study along with paleoclimate proxies from several other studies to identify the changes in provenance and erosion pattern as a response to climate excursions. The plot has been divided into three major climate stages, MIS 1, 2 and 3. MIS also known as OIS are periods of time in the past identified by changes in the oxygen isotope ratio in marine sediments. The odd numbers 1, 3... refer to warmer and even numbers 2, 4… refers to cooler periods. Further we also have Heinrich events (H1, H2, H3) and Younger Dryas which were basically cold periods and B/A period characterized by rapid warming and retreat of ice sheets. Considering all these climatic parameters, we see no significant changes during the MIS 3 stage which is mainly because our data only goes back till 35 kyr. Within the cold period MIS 2, chemical weathering and carbonate content starts to increase around 26 kyr. The changes in chemical weathering can be explained by changes in continental weathering pattern and/or shelf weathering of exposed sediments, due to low stand sea level during glacial period.

During glacial periods excessive glacial grinding and abrasion can lead to fine grained sediments, which can promote more water-rock interaction thereby increasing chemical weathering. A similar process is suggested by Lupker et al. (2013). However, an increase in chemical weathering during cold regime with weak SW monsoon is in contrast with the available data on intense weathering in warmer conditions. The other possibility is the weathering of the shelf sediments that are generally exposed during glacial periods when the sea level declines (Wan et al., 2016). Interestingly we also observe a significant increase in carbonate content ($CaCO_3$) at the same time. Similar increase in carbonate content during glacial periods is also observed by Peketi et al. (2020) and Sebastian et al. (2023). This increase in carbonate content can come from biogenic and/or detrital sources. Although there are studies that suggest increased productivity during glacial time (Verma et al., 2022) however, productivity alone cannot account for such huge increase in carbonate content. So the additional carbonate can come from the shelf erosion of exposed sediments during glacial low-stands as these shelves have large carbonate deposits. Thus shelf weathering plays an important role in describing weathering patterns particularly during glacial phases.

4 Conclusions

The sediment core VM29-17 from western BoB preserves the erosional record of Himalayas relative to Peninsular India for the last 35 kyrs. High-resolution chronology and Sr-Nd isotope data show an increased sediment supply from Himalayan rivers since ~15 kyr which is synchronous to the B/A warm phase. During the B/A phase, sudden warming caused the glacial cover over the Himalayas to retreat and expose surface rocks for weathering. At the same time, SW monsoon grew stronger and intense precipitation over the Himalayas led to more weathering and erosion in these regions. The isotopic analyses do not show a significant change in sediment provenance during LGM (18-24 kyr) rather low Sr isotopic ratio and high Nd ratios are observed for a broad range of ~15 to 30 kyr BP. This is consistent with the study by Lambeck et al., 2014, where the global sea level decreased significantly over 30 to 15 kyr implying that nearly stable ice sheet cover was observed throughout this period.

The post-glacial increase in sediment supply from Himalayas is synchronous with increase in the chemical erosion which is observed by CIA and K/Al ratio. The increasing values of CIA do not compensate for provenance change alone, hence, there has been intensification in weathering due to the strengthening of the SW monsoon which is also observed by nearby cores MD161-8 (Peketi et al., 2020) and U1445 (Lee et al., 2022). Increase in chemical and physical erosion in the Himalayan basin is possibly linked to efficient transport of locked sediments during glacial periods.

References

Ahmad, S.M., Anil Babu, G., Padmakumari, V.M., Dayal, A.M., Sukhija, B.S. and Nagabhushanam, P., 2005. Sr, Nd isotopic evidence of terrigenous flux variations in the Bay of Bengal: Implications of monsoons during the last∼ 34,000 years. *Geophysical Research Letters*, *32*(22).

Ahmad, S.M., Padmakumari, V.M. and Babu, G.A., 2009. Strontium and neodymium isotopic compositions in sediments from Godavari, Krishna and Pennar rivers. *Current science*, pp.1766-1769.

Andersen, K.K., Svensson, A., Johnsen, S.J., Rasmussen, S.O., Bigler, M., Röthlisberger, R., Ruth, U., Siggaard-Andersen, M.L., Steffensen, J.P., Dahl-Jensen, D. and Vinther, B.M., 2006. The Greenland ice core chronology 2005, 15–42 ka. Part 1: constructing the time scale. *Quaternary Science Reviews*, *25*(23-24), pp.3246-3257.

Bastia, F., Equeenuddin, S.M., Roy, P.D. and Hernández-Mendiola, E., 2020. Geochemical signatures of surface sediments from the Mahanadi river basin (India): Chemical weathering, provenance, and tectonic settings. Geological Journal, 55(7), pp.5294-5307.

Berger, A. and Loutre, M.F., 1991. Insolation values for the climate of the last 10 million years. *Quaternary Science Reviews*, *10*(4), pp.297-317.

Bluth, G.J. and Kump, L.R., 1994. Lithologic and climatologic controls of river chemistry. *Geochimica et Cosmochimica Acta*, *58*(10), pp.2341-2359.

Boral, S., Peucker-Ehrenbrink, B., Hemingway, J.D., Sen, I.S., Galy, V. and Fiske, G.J., 2021. Controls on short-term dissolved $^{87}Sr/^{86}Sr$ variations in large rivers: Evidence from the Ganga–Brahmaputra. *Earth and Planetary Science Letters*, *566*, p.116958.

Borghini, G., Rampone, E., Zanetti, A., Class, C., Cipriani, A., Hofmann, A.W. and Goldstein, S.L., 2016. Pyroxenite layers in the Northern Apennines' upper mantle (Italy)—generation by pyroxenite melting and melt infiltration. *Journal of Petrology*, *57*(4), pp.625-653.

Cai, M., Xu, Z., Clift, P.D., Lim, D., Khim, B.K., Yu, Z., Kulhanek, D.K., Li, T., Chen, H. and Sun, R., 2019. Depositional history and Indian summer monsoon controls on the silicate weathering of sediment transported to the eastern Arabian Sea: Geochemical records from IODP Site U1456 since 3.8 Ma. *Geochemistry, Geophysics, Geosystems*, *20*(9), pp.4336-4353.

Colin, C., Turpin, L., Bertaux, J., Desprairies, A. and Kissel, C., 1999. Erosional history of the Himalayan and Burman ranges during the last two glacial–interglacial cycles. *Earth and Planetary Science Letters*, *171*(4), pp.647-660.

Das, A. and Krishnaswami, S., 2007. Elemental geochemistry of river sediments from the Deccan Traps, India: implications to sources of elements and their mobility during basalt–water interaction. *Chemical Geology*, *242*(1-2), pp.232-254.

Dutta, K., Bhushan, R. and Somayajulu, B., 2001. ΔR correction values for the northern Indian Ocean. *Radiocarbon*, *43*(2A), pp.483-488.

France-Lanord, C. and Derry, L.A., 1997. Organic carbon burial forcing of the carbon cycle from Himalayan erosion. *Nature*, *390*(6655), pp.65-67.

Galy, V., François, L., France-Lanord, C., Faure, P., Kudrass, H., Palhol, F. and Singh, S.K., 2008. C4 plants decline in the Himalayan basin since the Last Glacial Maximum. Quaternary Science Reviews, 27(13-14), pp.1396-1409.

Garzanti, E., Andó, S., France-Lanord, C., Censi, P., Vignola, P., Galy, V. and Lupker, M., 2011. Mineralogical and chemical variability of fluvial sediments 2. Suspended-load silt (Ganga–Brahmaputra, Bangladesh). *Earth and Planetary Science Letters*, *302*(1-2), pp.107-120.

Goodbred Jr, S.L. and Kuehl, S.A., 2000. Enormous Ganges-Brahmaputra sediment discharge during strengthened early Holocene monsoon. *Geology*, *28*(12), pp.1083-1086.

Goswami, V., Singh, S.K., Bhushan, R. and Rai, V.K., 2012. Temporal variations in $^{87}Sr/^{86}Sr$ and ε_{Nd} in sediments of the southeastern Arabian Sea: Impact of monsoon and surface water circulation. *Geochemistry, Geophysics, Geosystems*, *13*(1).

Hilton, R.G. and West, A.J., 2020. Mountains, erosion and the carbon cycle. *Nature Reviews Earth & Environment*, *1*(6), pp.284-299.

Jacobsen, S.B. and Wasserburg, G.J., 1984. Sm-Nd isotopic evolution of chondrites and achondrites, II. *Earth and Planetary Science Letters*, *67*(2), pp.137-150.

Kessarkar, P.M., Rao, V.P., Ahmad, S.M., Patil, S.K., Kumar, A.A., Babu, G.A., Chakraborty, S. and Rajan, R.S., 2005. Changing sedimentary environment during the Late Quaternary: Sedimentological and isotopic evidence from the distal Bengal Fan. Deep Sea Research Part I: Oceanographic Research Papers, 52(9), pp.1591-1615.

Lambeck, K., Rouby, H., Purcell, A., Sun, Y. and Sambridge, M., 2014. Sea level and global ice volumes from the Last Glacial Maximum to the Holocene. *Proceedings of the National Academy of Sciences*, *111*(43), pp.15296-15303.

Lee, J., Kim, S., Ikehara, M., Horikawa, K., Asahara, Y., Yoo, C.M. and Khim, B.K., 2022. Indian monsoon variability in the Mahanadi Basin over the last two glacial cycles and its implications on the Indonesian throughflow. Geoscience Frontiers, p.101483.

Liu, S., Ye, W., Chen, M.T., Pan, H.J., Cao, P., Zhang, H., Khokiattiwong, S., Kornkanitnan, N. and Shi, X., 2021. Millennial-scale variability of Indian summer monsoon during the last 42 kyr: Evidence based on foraminiferal Mg/Ca and oxygen isotope records from the central Bay of Bengal. Palaeogeography, Palaeoclimatology, Palaeoecology, 562, p.110112.

Lupker, M., France-Lanord, C., Galy, V., Lavé, J. and Kudrass, H., 2013. Increasing chemical weathering in the Himalayan system since the Last Glacial Maximum. Earth and Planetary Science Letters, 365, pp.243-252.

Mahoney, J.J., Sheth, H.C., Chandrasekharam, D. and Peng, Z.X., 2000. Geochemistry of flood basalts of the Toranmal section, northern Deccan Traps, India: implications for regional Deccan stratigraphy. *Journal of Petrology*, *41*(7), pp.1099-1120.

Mandal, S.K., Lupker, M., Burg, J.P., Valla, P.G., Haghipour, N. and Christl, M., 2015. Spatial variability of ^{10}Be-derived erosion rates across the southern Peninsular Indian escarpment: A key to landscape evolution across passive margins. *Earth and Planetary Science Letters*, *425*, pp.154-167.

Milliman, J.D. and Syvitski, J.P., 1992. Geomorphic/tectonic control of sediment discharge to the ocean: the importance of small mountainous rivers. *The journal of Geology*, *100*(5), pp.525-544.

Mohanty, P.K., Pradhan, Y., Nayak, S.R., Panda, U.S. and Mohapatra, G.N., 2008. Sediment dispersion in the Bay of Bengal. *Monitoring and modelling lakes and coastal environments*, pp.50-78.

Naidu, P.D. and Govil, P., 2010. New evidence on the sequence of deglacial warming in the tropical Indian Ocean. Journal of Quaternary Science, 25(7), pp.1138-1143.

Nesbitt, H. and Young, G.M., 1982. Early Proterozoic climates and plate motions inferred from major element chemistry of lutites. nature, 299(5885), pp.715-717.

Pattan, J.N., Pratibhan, G., Babu, C.P., Khadge, N.H., Paropkari, A.L. and Kodagali, V.N., 2008. A note on geochemistry of surface sediments from Krishna-Godavari basin, East Coast of India. *Geological Society of India*, *71*(1), pp.107-114.

Peketi, A., Mazumdar, A., Pillutla, S.P.K., Rai, V.K., Sawant, B. and Chaitanya, A.V.S., 2020. Monsoon rainfall and contrasting source rocks influenced sediment composition of peninsular basins along the east coast of India (western Bay of Bengal). Marine and Petroleum Geology, 118, p.104433.

Peketi, A., Mazumdar, A., Pillutla, S.P.K., Sawant, B. and Gupta, H., 2021. Climatic and tectonic control on the Bengal fan sedimentation since the Pliocene. Geochemistry, Geophysics, Geosystems, 22(3), p.e2020GC009448.

Prasanna Kumar, S., Muraleedharan, P.M., Prasad, T.G., Gauns, M., Ramaiah, N., De Souza, S.N., Sardesai, S. and Madhupratap, M., 2002. Why is the Bay of Bengal less productive during summer monsoon compared to the Arabian Sea?. *Geophysical Research Letters*, *29*(24), pp.88-1.

Rahaman, W., Singh, S.K., Sinha, R. and Tandon, S.K., 2009. Climate control on erosion distribution over the Himalaya during the past~ 100 ka. *Geology*, *37*(6), pp.559-562.

Raymo, M.E. and Ruddiman, W.F., 1992. Tectonic forcing of late Cenozoic climate. *Nature*, *359*(6391), pp.117-122.

Samanta, A., Tripathy, G.R., Nath, B.N., Bhushan, R., Panchang, R., Bharti, N. and Shrivastava, A., 2022. Holocene variability in chemical weathering and ocean redox state: A reconstruction using sediment geochemistry of the Arabian Sea. *Journal of Asian Earth Sciences*, *224*, p.105029.

Sebastian, T., Nath, B.N., Miriyala, P., Linsy, P. and Kocherla, M., 2023. Climatic control on detrital sedimentation in the continental margin off Chennai, western Bay of Bengal–A 42 kyr record. *Palaeogeography, Palaeoclimatology, Palaeoecology*, *609*, p.111313.

Sengupta, D., Bharath Raj, G.N. and Shenoi, S.S.C., 2006. Surface freshwater from Bay of Bengal runoff and Indonesian throughflow in the tropical Indian Ocean. *Geophysical Research Letters*, *33*(22).

Singh, S.K., Rai, S.K. and Krishnaswami, S., 2008. Sr and Nd isotopes in river sediments from the Ganga Basin: sediment provenance and spatial variability in physical erosion. *Journal of Geophysical Research: Earth Surface*, *113*(F3).

Stuiver, M. and Reimer, P.J., 1993. Extended ^{14}C data base and revised CALIB 3.0 14C age calibration program. *Radiocarbon*, *35*(1), pp.215-230.

Tripathy, G.R., Singh, S.K., Bhushan, R. and Ramaswamy, V., 2011. Sr–Nd isotope composition of the Bay of Bengal sediments: impact of climate on erosion in the Himalaya. Geochemical Journal, 45(3), pp.175-186.

Tripathy, G.R., Singh, S.K. and Ramaswamy, V., 2014. Major and trace element geochemistry of Bay of Bengal sediments: Implications to provenances and their controlling factors. *Palaeogeography, Palaeoclimatology, Palaeoecology*, *397*, pp.20-30.

Verma, K., Singh, A.D., Singh, P., Singh, H., Satpathy, R.K., Uddandam, P.R. and Naidu, P.D., 2022. Monsoon-related changes in surface hydrography and productivity in the Bay of Bengal over the last 45 kyr BP. *Palaeogeography, Palaeoclimatology, Palaeoecology*, *589*, p.110844.

Vinayachandran, P.N., Shankar, D., Vernekar, S., Sandeep, K.K., Amol, P., Neema, C.P. and Chatterjee, A., 2013. A summer monsoon pump to keep the Bay of Bengal salty. *Geophysical Research Letters*, *40*(9), pp.1777-1782.

Von Blanckenburg, F., Bouchez, J., Ibarra, D.E. and Maher, K., 2015. Stable runoff and weathering fluxes into the oceans over Quaternary climate cycles. *Nature Geoscience*, *8*(7), pp.538-542.

West, A.J., Galy, A. and Bickle, M., 2005. Tectonic and climatic controls on silicate weathering. *Earth and Planetary Science Letters*, *235*(1-2), pp.211-228.

Wan, S., Clift, P.D., Zhao, D., Hovius, N., Munhoven, G., France-Lanord, C., Wang, Y., Xiong, Z., Huang, J., Yu, Z. and Zhang, J., 2017. Enhanced silicate weathering of tropical shelf sediments exposed during glacial lowstands: A sink for atmospheric CO2. *Geochimica et Cosmochimica Acta*, *200*, pp.123-144.

Wang, Y.J., Cheng, H., Edwards, R.L., An, Z.S., Wu, J.Y., Shen, C.C. and Dorale, J.A., 2001. A high-resolution absolute-dated late Pleistocene monsoon record from Hulu Cave, China. *Science*, *294*(5550), pp.2345-2348.

White, A.F., Blum, A.E., Bullen, T.D., Vivit, D.V., Schulz, M. and Fitzpatrick, J., 1999. The effect of temperature on experimental and natural chemical weathering rates of granitoid rocks. *Geochimica et Cosmochimica Acta*, *63*(19-20), pp.3277-3291.

Yuan, D., Cheng, H., Edwards, R.L., Dykoski, C.A., Kelly, M.J., Zhang, M., Qing, J., Lin, Y., Wang, Y., Wu, J. and Dorale, J.A., 2004. Timing, duration, and transitions of the last interglacial Asian monsoon. *Science*, *304*(5670), pp.575-578.

Annexure

Table A1 *Concentrations (in wt%) of C_{inorg}, $CaCO_3$, weight loss during decarbonation using 0.6 N HCl and ashing at 550°C for the VM29-17 core.*

Sample ID	Depth (cm)		Age	C_{inorg}	$CaCO_3$	Decarbonation	LOI 550	CIA*
	From	To	kyr	wt %		wt loss %		
17PC-01	0	2	0.0	0.22	1.82	24	11.1	85
17PC-02	5	7	0.1	0.21	1.78	26	13.6	85
17PC-03	10	12	0.3	0.24	1.98	20	12.2	85
17PC-04	15	17	0.4	0.17	1.38	22	9.8	85
17PC-05	20	22	0.5	0.25	2.12	21	13.8	84
17PC-06	25	27	0.7	0.50	4.14	23	10.2	85
17PC-07	30	31	0.9	0.40	3.33	22	12.4	84
17PC-08	35	36	1.2	0.37	3.08	21	11.7	85
17PC-09	40	41	1.5	0.68	5.69	24	13.8	85
17PC-10	50	51	2.0	0.31	2.60	20	11.7	85
17PC-11	55	56	2.2	0.22	1.82	20	10.2	84
17PC-12	60	61	2.5	0.57	4.74	22	11.6	84
17PC-13	65	66	2.7	0.37	3.12	21	9.7	84
17PC-14	70	71	3.0	0.26	2.18	20	12.1	84
17PC-15	75	76	3.3	0.36	3.04	21	9.7	84
17PC-16	84.5	86.5	3.6	0.74	6.20	22	10.0	84
17PC-17	90	91	3.8	0.24	2.00	23	12.5	83
17PC-18	95	96	4.0	0.34	2.85	24	9.3	82
17PC-19	100	101	4.2	0.66	5.49	23	8.7	82
17PC-20	105	106	4.4	0.65	5.44	18	10.3	81
17PC-21	110	111	4.6	1.02	8.54	23	8.8	79
17PC-22	115	117	4.8	0.67	5.59	24	11.6	83
17PC-23	120	121	5.0	0.46	3.85	21	9.1	83
17PC-24	125	126	5.2	0.41	3.44	20	11.1	83
17PC-25	130	131	5.4	0.62	5.20	21	10.3	82
17PC-26	135	136	5.6	0.58	4.85	22	8.9	81
17PC-27	140	141	5.8	2.60	21.65	31	5.9	75
17PC-28	145	146	6.0	0.34	2.83	20	9.4	83
17PC-29	150	151	6.2	0.53	4.43	21	11.6	83
17PC-30	155	156	6.9	0.62	5.17	22	10.9	83
17PC-31	165	166	8.2	0.79	6.62	24	10.2	82
17PC-32	170	171	8.9	0.84	7.03	24	9.5	81
17PC-33	175	176	9.5	1.20	9.97	25	9.4	80
17PC-34	180	181	10.2	0.56	4.64	20	10.6	83
17PC-35	185	186	10.8	1.45	12.05	27	9.2	82
17PC-36	190	191	11.5	1.54	12.83	28	10.5	81
17PC-37	195.5	196.5	12.0	2.34	19.47	32	10.0	81
17PC-38	200	201	12.4	2.48	20.63	32	9.1	81

17PC-39	205	206	12.8	2.93	24.43	36	10.8	81
17PC-40	210	211	13.2	2.42	20.19	41	9.3	81
17PC-41	215	216	14.3	2.64	21.96	37	9.9	81
17PC-42	220	221	15.3	2.44	20.30	33	9.2	77
17PC-43	226	227	16.5	2.04	16.98	31	9.0	79
17PC-44	230	231	17.4	1.61	13.44	28	7.7	78
17PC-45	235	236	17.9	2.08	17.33	30	8.6	78
17PC-46	240	241	18.4	1.62	13.49	29	9.3	78
17PC-47	245	246	18.9	1.68	13.97	35	8.8	78
17PC-48	250	251	19.4	2.10	17.54	31	9.7	77
17PC-49	255	256	20.0	1.68	14.00	29	8.6	77
17PC-50	260	261	20.5	1.76	14.66	32	8.3	77
17PC-51	265	266	21.0	2.37	19.79	33	10.3	77
17PC-52	270	271	21.5	1.73	14.42	32	7.2	77
17PC-53	275	276	22.0	1.61	13.40	28	5.4	76
17PC-54	280	281	22.4	1.54	12.82	29	7.6	76
17PC-55	290	291	23.4	1.64	13.69	29	7.8	76
17PC-56	295	296	23.8	1.80	14.97	30	9.3	76
17PC-57	300	301	24.3	1.26	10.48	27	7.9	76
17PC-58	305	306	24.6	1.13	9.44	26	8.3	76
17PC-59	310	311	25.0	1.04	8.66	26	6.5	75
17PC-60	315	316	25.3	0.96	7.97	24	6.8	75
17PC-61	320	321	25.7	0.38	3.14	20	7.2	74
17PC-62	325	326	26.0	0.65	5.42	20	7.5	74
17PC-63	335	336	26.7	0.82	6.80	27	11.1	76
17PC-64	340	341	27.1	0.57	4.78	22	6.6	77
17PC-65	345	346	27.4	1.27	10.54	27	10.5	76
17PC-66	349.5	350	27.8	1.43	11.92	27	6.6	77
17PC-67	355	356	28.1	1.24	10.33	24	9.0	76
17PC-68	360	361	28.5	1.04	8.66	25	7.6	76
17PC-69	365	366	28.8	1.08	8.96	26	6.5	78
17PC-70	370	371	29.2	0.46	3.82	26	7.4	77
17PC-71	375	376	29.5	1.01	8.43	25	10.6	78
17PC-72	380	381	29.9	1.02	8.47	27	9.5	77
17PC-73	385	386	30.2	0.58	4.79	27	11.4	78
17PC-74	390	391	30.6	0.93	7.78	25	6.7	77
17PC-75	395	396	30.9	1.02	8.49	25	9.3	78
17PC-76	400	401	31.3	0.71	5.92	26	10.4	77
17PC-77	405	406	31.6	0.51	4.25	22	8.7	76
17PC-78	410	411	32.0	0.52	4.30	15	4.4	72
17PC-79	415	416	32.3	0.58	4.82	24	9.9	77
17PC-80	420	421	32.7	0.51	4.26	23	7.0	76
17PC-81	425	426	33.0	0.62	5.18	22	5.8	76
17PC-82	430	431	33.4	0.66	5.49	24	10.3	77
17PC-83	435	436	33.7	0.47	3.91	23	9.6	75
17PC-84	440	441	34.1	0.82	6.79	23	9.6	76

17PC-85	445	446	34.4	0.53	4.39	21	10.0	76
17PC-86	450	451	34.8	0.59	4.90	21	8.3	76
17PC-87	455	456	35.1	0.66	5.47	15	3.3	70
17PC-88	460	461	35.5	0.55	4.56	19	5.4	73

Table A2 *Major and trace elemental, and Sr-Nd isotopic data for the VM29-17 sediments.*

Sample ID	Depth	Age	Al	Na	Mg	Si	K	Ca	Ti	Fe	CIA	V	Cr	Mn	Co	Ni	Cu	Zn	Rb	Sr	Ba	$^{87}Sr/^{86}Sr$	ε_{Nd}
	(cm)	(kyr)	(wt %)									(µg/g)											
17PC-01	1	0.0	9.21	0.30	0.99	25.02	1.84	0.14	0.63	5.36	83.59	151	70	1938	11	59	46	81	18	19	115		
17PC-02	6	0.1	8.93	0.27	0.99	24.07	1.78	0.13	0.60	5.29	83.85	105	70	245	11	57	62	108	25	25	132	0.7423	-15.91
17PC-03	11	0.3	9.08	0.28	1.03	24.11	1.84	0.13	0.60	5.43	83.70	127	76	633	16	72	67	112	465	108	679		
17PC-04	16	0.4	9.06	0.30	1.00	25.07	1.87	0.14	0.62	5.49	83.18												
17PC-05	21	0.5	8.73	0.30	1.00	24.29	1.84	0.13	0.60	5.40	82.97	119	65	349	12	62	60	165	35	33	55		
17PC-06	26	0.7	9.10	0.31	1.00	25.17	1.88	0.13	0.62	5.17	83.13	128	79	427	14	70	71	93	227	65	364	0.7427	-15.92
17PC-07	30.5	0.9	9.06	0.31	0.98	24.76	1.90	0.13	0.61	5.07	83.07	118	67	262	10	59	64	80	29	26	39		
17PC-08	35.5	1.2	9.21	0.30	1.00	24.83	1.88	0.13	0.60	5.19	83.47	106	71	252	10	56	60	72	32	20	64		
17PC-09	40.5	1.5	8.35	0.26	0.90	24.75	1.66	0.13	0.60	4.68	83.68	129	77	119	10	63	77	94	17	16	84	0.7416	-16.22
17PC-10	50.5	2.0	9.21	0.29	0.97	25.02	1.95	0.10	0.60	5.13	83.46	118	77	279	11	63	69	100	30	20	81		
17PC-11	55.5	2.2	9.24	0.31	1.04	24.81	1.97	0.12	0.58	5.43	83.05												
17PC-12	60.5	2.5	9.31	0.31	1.04	24.66	2.01	0.14	0.58	5.14	82.76	108	65	383	11	62	58	87	124	46	202		
17PC-13	65.5	2.7	9.00	0.31	0.95	24.79	1.98	0.14	0.58	4.96	82.38	110	66	388	11	62	57	63	128	48	245		
17PC-14	70.5	3.0	9.12	0.33	0.98	24.79	2.01	0.14	0.57	4.87	82.32	114	67	274	11	61	59	126	20	18	37		
17PC-15	75.5	3.3	8.90	0.30	0.93	24.86	2.01	0.12	0.56	4.89	82.41	99	68	278	11	60	59	120	66	30	132	0.7413	-16.91
17PC-16	85.5	3.6	9.31	0.31	1.06	25.07	2.06	0.12	0.57	5.02	82.66	115	78	304	12	68	65	93	42	32	82		
17PC-17	90.5	3.8	9.03	0.33	0.96	24.53	2.03	0.14	0.56	4.63	82.01												
17PC-18	95.5	4.0	9.44	0.38	1.02	25.62	2.25	0.16	0.56	4.69	81.00												
17PC-19	100.5	4.2	9.07	0.40	0.93	25.71	2.22	0.16	0.56	4.38	80.36	112	66	202	10	55	60	75	24	21	57		
17PC-20	105.5	4.4	9.26	0.42	1.00	25.59	2.40	0.17	0.52	4.34	79.58												
17PC-21	110.5	4.6	8.62	0.53	0.83	27.24	2.39	0.24	0.52	3.66	76.91	129	78	135	8	50	44	8	33	31	79	0.7497	-18.20
17PC-22	116	4.8	9.07	0.33	0.92	24.88	2.12	0.13	0.56	4.57	81.79	104	65	208	9	51	36	57	37	25	46		
17PC-23	120.5	5.0	9.34	0.33	1.01	25.41	2.19	0.13	0.57	4.79	81.82												
17PC-24	125.5	5.2	9.15	0.34	1.00	25.23	2.18	0.14	0.55	4.56	81.34	125	82	182	9	63	56	26	31	24	85	0.7438	-16.58
17PC-25	130.5	5.4	9.14	0.37	0.98	25.46	2.21	0.17	0.55	4.63	80.69												
17PC-26	135.5	5.6	9.18	0.47	0.90	26.63	2.29	0.21	0.54	4.03	79.23	100	63	197	9	48	38	72	43	41	82		

17PC-27	140.5	5.8	7.27	0.74	0.73	29.78	2.27	0.45	0.51	3.55	70.55	60	50	257	10	35	24	70	126	103	297	0.7442	-16.41
17PC-28	145.5	6.0	9.32	0.33	1.01	25.28	2.15	0.17	0.60	5.08	81.61	117	73	235	11	62	41	77	23	22	55		
17PC-29	150.5	6.2	8.64	0.31	0.97	24.82	2.03	0.13	0.52	5.35	81.61	94	72	622	14	66	38	179	32	27	154	0.7393	-16.39
17PC-30	155.5	6.9	9.31	0.34	0.94	25.30	2.14	0.13	0.55	4.68	81.98												
17PC-31	165.5	8.2	9.21	0.42	0.93	25.78	2.25	0.17	0.53	4.56	80.19												
17PC-32	170.5	8.9	9.35	0.49	0.95	26.24	2.37	0.19	0.53	4.02	79.13	111	70	303	12	58	42	62	187	73	332		
17PC-33	175.5	9.5	9.19	0.53	0.88	26.38	2.34	0.22	0.53	3.77	78.41	101	66	160	9	51	41	165	25	27	112	0.7367	-15.59
17PC-34	180.5	10.2	9.28	0.39	0.98	25.46	2.16	0.16	0.54	4.67	81.13	100	74	281	11	60	44	83	48	27	91		
17PC-35	185.5	10.8	9.19	0.39	1.00	25.81	2.24	0.17	0.55	4.89	80.46												
17PC-36	190.5	11.5	9.01	0.44	1.07	25.60	2.30	0.19	0.55	4.64	79.25	104	66	307	14	61	53	96	19	28	94	0.7337	-15.99
17PC-37	196	12.0	8.96	0.43	1.12	25.57	2.22	0.20	0.55	4.79	79.53	118	68	412	15	68	50	83	13	28	66		
17PC-38	200.5	12.4	9.01	0.44	1.21	25.54	2.28	0.21	0.57	4.91	79.19												
17PC-39	205.5	12.8	8.71	0.45	1.10	25.40	2.20	0.21	0.56	4.50	78.87												
17PC-40	210.5	13.2	8.63	0.46	1.09	25.58	2.16	0.24	0.57	4.62	78.56	141	78	392	17	79	62	184	23	40	216	0.7317	-15.51
17PC-41	215.5	14.3	8.94	0.51	1.13	25.83	2.24	0.25	0.57	4.44	78.22												
17PC-42	220.5	15.3	8.12	0.64	1.21	27.28	2.33	0.36	0.61	4.77	74.11	168	95	932	27	89	60	144	453	170	1020	0.7274	-14.38
17PC-43	226.5	16.5	8.80	0.63	1.29	26.42	2.33	0.32	0.59	4.56	76.01	133	72	463	17	68	50	83	157	93	337		
17PC-44	230.5	17.4	8.60	0.66	1.11	26.91	2.36	0.33	0.58	4.10	75.11												
17PC-45	235.5	17.9	8.52	0.68	1.16	26.65	2.37	0.34	0.58	4.16	74.68	129	64	402	15	62	47	50	28	59	83		
17PC-46	240.5	18.4	8.85	0.69	1.28	26.04	2.37	0.35	0.56	4.09	75.26	80	54	298	12	48	34	96	10	32	47	0.7275	-14.37
17PC-47	245.5	18.9	8.71	0.70	1.11	26.90	2.36	0.34	0.57	3.83	74.94	125	63	375	15	57	44	86	62	72	116		
17PC-48	250.5	19.4	8.46	0.73	1.07	26.31	2.34	0.38	0.56	3.60	73.93	125	62	360	14	56	53	97	65	67	135		
17PC-49	255.5	20.0	8.48	0.72	1.05	26.75	2.40	0.38	0.57	3.75	73.76	166	79	347	16	68	51	101	40	47	83	0.7304	-15.36
17PC-50	260.5	20.5	8.49	0.74	1.11	27.17	2.40	0.38	0.58	3.97	73.63	133	61	397	17	56	42	71	59	64	125		
17PC-51	265.5	21.0	8.39	0.73	1.16	26.00	2.35	0.38	0.55	3.85	73.68	141	76	449	17	64	54	121	66	80	72		
17PC-52	270.5	21.5	8.40	0.75	1.01	27.31	2.35	0.38	0.57	3.86	73.57	92	55	333	13	47	35	189	36	65	64	0.7292	-15.24
17PC-53	275.5	22.0	8.71	0.80	1.28	27.22	2.56	0.43	0.57	4.41	72.64												
17PC-54	280.5	22.4	8.69	0.84	1.13	27.36	2.48	0.45	0.60	3.81	72.50												
17PC-55	290.5	23.4	8.43	0.83	1.14	27.33	2.50	0.45	0.59	4.10	71.87												
17PC-56	295.5	23.8	8.58	0.81	1.24	26.15	2.52	0.43	0.56	3.93	72.43	128	63	467	15	56	33	116	292	120	692		

17PC-57	300.5	24.3	8.63	0.86	1.06	27.54	2.52	0.45	0.58	3.50	71.98	132	65	293	11	51	40	118	133	84	320	0.7292	-14.81
17PC-58	305.5	24.6	8.79	0.86	1.01	27.05	2.58	0.42	0.54	3.39	72.33	116	52	259	11	40	37	111	87	81	169		
17PC-59	310.5	25.0	8.83	0.91	0.98	27.94	2.70	0.49	0.57	3.10	71.14	113	54	251	10	40	32	423	26	51	41		
17PC-60	315.5	25.3	9.16	0.97	0.96	27.81	2.71	0.50	0.54	2.74	71.37	88	52	197	8	34	23	96	12	33	22	0.7307	-15.86
17PC-61	320.5	25.7	8.83	1.02	0.90	28.19	2.67	0.52	0.52	2.56	70.20												
17PC-62	325.5	26.0	8.77	1.04	0.86	28.53	2.67	0.55	0.52	2.40	69.78	89	49	193	6	30	12	55	110	85	205		
17PC-63	335.5	26.7	8.29	0.80	0.92	26.30	2.45	0.41	0.54	3.00	72.31	136	68	242	11	44	38	112	21	28	42	0.7310	-15.22
17PC-64	340.5	27.1	8.94	0.78	0.92	26.99	2.55	0.39	0.55	3.50	73.63												
17PC-65	345.5	27.4	8.73	0.82	0.96	26.51	2.58	0.39	0.55	3.27	72.75	108	54	327	11	42	19	91	127	80	346		
17PC-66	349.75	27.8	8.93	0.80	0.99	27.21	2.56	0.41	0.57	3.31	73.23	119	53	333	12	43	21	68	81	95	223		
17PC-67	355.5	28.1	8.81	0.84	1.05	26.61	2.69	0.42	0.55	3.42	72.09	137	68	269	13	50	22	76	47	54	89	0.7335	-15.92
17PC-68	360.5	28.5	8.90	0.78	0.99	27.19	2.65	0.38	0.58	3.48	73.26												
17PC-69	365.5	28.8	8.73	0.68	1.06	26.63	2.41	0.33	0.57	4.12	74.98												
17PC-70	370.5	29.2	8.78	0.76	0.98	26.72	2.52	0.39	0.56	3.46	73.57	115	58	357	12	43	35	254	66	67	177		
17PC-71	375.5	29.5	8.48	0.68	1.03	26.09	2.32	0.34	0.56	3.85	74.78												
17PC-72	380.5	29.9	8.07	0.67	0.92	26.61	2.30	0.31	0.54	4.02	74.29	109	63	460	18	48	48	214	261	137	655	0.7302	-14.50
17PC-73	385.5	30.2	8.43	0.68	0.95	26.29	2.35	0.31	0.55	3.56	74.79	124	56	287	13	44	42	124	21	41	26		
17PC-74	390.5	30.6	8.58	0.68	1.00	27.06	2.47	0.31	0.55	4.06	74.63												
17PC-75	395.5	30.9	8.78	0.70	0.97	26.50	2.49	0.30	0.55	3.59	74.86	175	78	326	16	61	61	142	85	60	201	0.7334	-15.38
17PC-76	400.5	31.3	8.98	0.77	0.90	26.45	2.58	0.35	0.53	3.00	74.02	110	53	203	9	35	24	68	41	55	41		
17PC-77	405.5	31.6	8.96	0.85	0.81	27.52	2.75	0.40	0.54	2.39	72.32	107	61	159	6	31	19	71	20	18	10		
17PC-78	410.5	32.0	7.92	1.20	0.81	30.94	2.52	0.60	0.44	2.11	66.71	91	47	143	6	26	9	46	23	27	153	0.7382	-15.76
17PC-79	415.5	32.3	8.73	0.76	0.93	26.40	2.54	0.35	0.55	3.27	73.72	109	55	355	10	39	29	80	127	87	209		
17PC-80	420.5	32.7	8.81	0.77	0.91	26.88	2.67	0.38	0.54	3.16	72.97												
17PC-81	425.5	33.0	9.12	0.81	1.00	27.35	2.83	0.40	0.55	3.41	72.58	108	53	296	10	37	30	98	45	61	66		
17PC-82	430.5	33.4	9.00	0.78	1.00	26.20	2.62	0.35	0.53	3.25	73.82	133	67	228	9	43	38	88	23	30	74	0.7364	-16.00
17PC-83	435.5	33.7	8.74	0.85	0.95	26.74	2.71	0.41	0.52	3.20	71.85	107	50	292	9	33	28	86	19	45	17		
17PC-84	440.5	34.1	9.03	0.83	1.00	26.54	2.73	0.42	0.54	3.19	72.51	114	59	328	10	39	32	102	146	96	343		
17PC-85	445.5	34.4	8.96	0.81	0.99	26.57	2.74	0.41	0.53	3.23	72.54	110	64	303	9	37	30	95	23	44	42		
17PC-86	450.5	34.8	9.16	0.85	0.98	26.85	2.81	0.42	0.54	3.15	72.29	149	75	288	9	44	32	97	26	34	162	0.7376	-15.67

17PC-87	455.5	35.1	7.85	1.38	0.86	31.46	2.53	0.81	0.42	2.17	63.76	67	36	252	6	20	7	67	126	113	345		
17PC-88	460.5	35.5	8.94	1.15	0.93	29.13	2.91	0.62	0.49	2.40	68.11	127	58	170	7	31	13	66	43	38	230	0.7394	-16.01

Table A3 *Concentration data for the rare earth elements for the VM29-17 sediments.*

Sample ID	Depth (cm)	Age (kyr)	Sc	Y	La	Ce	Pr	Nd	Sm	Eu	Gd	Tb	Dy	Ho	Er	Tm	Yb	Lu	U
			(ppm or µg/g)																
17PC-01	1	0	8	4	5	13	19	4	0.95	0.17	0.79	0.12	0.70	0.16	0.55	0.11	0.62	0.12	1.14
17PC-02	6	0.1	6	4	7	16	20	5	1.31	0.19	1.08	0.16	0.79	0.19	0.70	0.09	0.65	0.13	1.32
17PC-03	11	0.3	53	27	48	90	149	31	5.24	1.07	4.28	0.65	4.14	0.85	2.51	0.44	2.93	0.39	2.97
17PC-05	21	0.5	8	5	9	20	30	7	1.32	0.23	1.04	0.14	0.89	0.18	0.61	0.11	0.63	0.12	1.40
17PC-06	26	0.7	29	14	22	43	71	16	2.57	0.49	2.24	0.36	2.22	0.47	1.44	0.25	1.85	0.27	2.39
17PC-07	30.5	0.9	5	3	7	14	22	5	0.95	0.16	0.79	0.11	0.56	0.13	0.36	0.06	0.44	0.07	1.04
17PC-08	35.5	1.2	4	3	5	11	20	5	0.91	0.16	0.77	0.11	0.63	0.13	0.51	0.06	0.50	0.10	1.09
17PC-09	40.5	1.5	6	5	6	9	21	5	1.17	0.21	0.97	0.15	0.89	0.20	0.62	0.10	0.68	0.10	1.15
17PC-10	50.5	2	6	4	5	12	18	4	0.88	0.15	0.78	0.12	0.71	0.17	0.48	0.08	0.52	0.09	1.14
17PC-12	60.5	2.5	14	7	13	28	46	10	1.68	0.29	1.39	0.21	1.26	0.25	0.83	0.14	0.94	0.15	1.48
17PC-13	65.5	2.7	17	9	16	30	51	12	1.95	0.41	1.59	0.25	1.63	0.34	0.92	0.17	1.05	0.19	1.66
17PC-14	70.5	3	3	3	5	12	15	4	0.76	0.12	0.59	0.09	0.46	0.12	0.37	0.06	0.40	0.05	1.06
17PC-15	75.5	3.3	9	4	7	17	21	5	1.40	0.24	1.18	0.18	0.67	0.26	0.79	0.10	0.61	0.09	1.51
17PC-16	85.5	3.6	8	5	10	26	33	8	1.40	0.25	1.16	0.16	0.95	0.19	0.63	0.10	0.68	0.11	1.57
17PC-19	100.5	4.2	4	3	5	15	20	5	0.93	0.13	0.69	0.10	0.59	0.13	0.42	0.06	0.46	0.07	1.37
17PC-21	110.5	4.6	4	7	11	23	39	10	1.91	0.25	1.59	0.23	1.25	0.27	0.75	0.13	0.97	0.15	1.65
17PC-22	116	4.8	4	3	8	19	27	7	1.11	0.17	0.85	0.11	0.53	0.12	0.39	0.06	0.39	0.06	1.09
17PC-24	125.5	5.2	5	7	6	9	22	5	1.16	0.19	0.96	0.20	1.27	0.28	0.81	0.17	1.06	0.13	1.27
17PC-26	135.5	5.6	6	5	11	19	39	9	1.41	0.25	1.20	0.16	0.86	0.19	0.52	0.08	0.56	0.09	1.46
17PC-27	140.5	5.8	10	16	20	44	68	16	3.69	0.70	2.91	0.45	2.52	0.65	1.69	0.23	1.93	0.28	2.70
17PC-28	145.5	6	5	4	11	24	41	10	1.85	0.21	1.23	0.17	0.81	0.17	0.49	0.08	0.49	0.08	1.42
17PC-29	150.5	6.2	7	6	9	22	28	7	1.63	0.31	1.55	0.18	1.08	0.31	0.90	0.11	0.73	0.12	1.20
17PC-32	170.5	8.9	16	13	25	49	82	18	3.10	0.55	2.39	0.36	2.14	0.44	1.27	0.21	1.47	0.19	2.02
17PC-33	175.5	9.5	3	6	12	33	39	10	1.91	0.35	1.63	0.23	1.01	0.20	0.85	0.09	0.72	0.11	1.36
17PC-34	180.5	10.2	6	4	8	17	29	6	1.11	0.21	0.98	0.13	0.71	0.16	0.49	0.08	0.56	0.09	1.17
17PC-36	190.5	11.5	4	4	5	15	15	4	1.06	0.17	1.14	0.14	0.60	0.19	0.71	0.08	0.55	0.06	1.24

17PC-37	196	12	3	4	6	17	24	6	1.14	0.17	0.82	0.12	0.67	0.14	0.44	0.08	0.50	0.07	1.27
17PC-40	210.5	13.2	9	10	16	35	54	13	2.87	0.46	2.00	0.30	1.56	0.34	1.08	0.17	1.09	0.16	1.61
17PC-42	220.5	15.3	51	39	63	130	214	48	8.54	1.70	6.78	0.98	6.32	1.31	3.92	0.58	4.15	0.62	4.02
17PC-43	226.5	16.5	17	14	24	51	80	18	3.20	0.61	2.38	0.37	2.31	0.45	1.42	0.24	1.59	0.23	2.23
17PC-45	235.5	17.9	4	6	12	32	41	10	1.63	0.25	1.21	0.16	0.83	0.21	0.58	0.09	0.64	0.10	1.44
17PC-46	240.5	18.4	2	3	5	21	16	4	0.90	0.18	1.05	0.11	0.42	0.14	0.45	0.06	0.53	0.07	1.25
17PC-47	245.5	18.9	7	7	15	36	51	11	2.00	0.35	1.55	0.21	1.26	0.25	0.83	0.10	0.81	0.13	1.93
17PC-48	250.5	19.4	7	6	14	37	47	10	1.83	0.32	1.29	0.18	0.97	0.22	0.59	0.10	0.70	0.11	1.85
17PC-49	255.5	20	6	8	12	23	44	9	1.82	0.25	1.41	0.21	1.18	0.30	0.87	0.12	1.03	0.16	1.96
17PC-50	260.5	20.5	6	6	14	35	46	10	1.74	0.31	1.38	0.18	1.02	0.22	0.65	0.09	0.70	0.11	1.71
17PC-51	265.5	21	6	6	14	46	43	10	1.70	0.27	1.31	0.17	0.90	0.19	0.63	0.12	0.73	0.10	1.87
17PC-52	270.5	21.5	3	6	13	35	39	9	1.86	0.30	1.56	0.17	0.93	0.21	1.04	0.11	0.78	0.10	1.75
17PC-56	295.5	23.8	24	24	41	72	146	31	5.73	1.07	4.13	0.65	3.92	0.78	2.12	0.34	2.29	0.33	2.31
17PC-57	300.5	24.3	13	15	22	43	71	16	3.05	0.64	2.52	0.37	2.40	0.47	1.52	0.24	1.73	0.31	2.16
17PC-58	305.5	24.6	7	8	16	39	58	13	2.24	0.41	1.80	0.25	1.26	0.27	0.71	0.15	0.88	0.16	1.88
17PC-59	310.5	25	2	8	11	43	36	8	1.59	0.24	1.31	0.19	1.22	0.26	0.91	0.15	0.99	0.15	1.93
17PC-60	315.5	25.3	2	11	6	43	21	5	1.79	0.30	1.71	0.23	1.76	0.44	1.25	0.23	1.53	0.16	2.09
17PC-62	325.5	26	9	13	19	52	64	14	2.70	0.46	2.27	0.32	1.90	0.42	1.30	0.20	1.46	0.23	2.29
17PC-63	335.5	26.7	4	7	6	13	19	4	1.07	0.17	1.07	0.16	0.98	0.25	0.76	0.12	0.93	0.15	1.68
17PC-65	345.5	27.4	10	14	24	53	79	18	3.31	0.53	2.35	0.35	2.24	0.45	1.21	0.23	1.47	0.22	2.17
17PC-66	349.75	27.8	10	17	23	59	84	19	3.47	0.64	3.06	0.44	2.75	0.58	1.64	0.29	1.76	0.27	2.57
17PC-67	355.5	28.1	5	10	12	26	41	10	1.87	0.24	1.75	0.25	1.75	0.36	1.15	0.17	1.40	0.19	2.29
17PC-70	370.5	29.2	7	2	4	14	14	3	0.69	0.12	0.59	0.09	0.50	0.11	0.34	0.07	0.47	0.08	1.44
17PC-72	380.5	29.9	25	17	32	62	101	23	3.94	0.83	3.60	0.48	2.99	0.76	2.00	0.37	2.21	0.31	2.72
17PC-73	385.5	30.2	2	3	8	26	28	6	1.02	0.17	0.85	0.10	0.50	0.12	0.33	0.05	0.43	0.08	1.53
17PC-75	395.5	30.9	10	12	14	29	49	11	2.15	0.36	1.90	0.26	1.87	0.39	1.41	0.22	1.43	0.23	2.09
17PC-76	400.5	31.3	2	4	10	34	32	8	1.35	0.21	1.01	0.12	0.60	0.14	0.42	0.06	0.46	0.08	1.72
17PC-77	405.5	31.6	1	6	8	36	28	7	1.21	0.19	1.10	0.15	0.88	0.20	0.71	0.13	0.90	0.11	2.01
17PC-78	410.5	32	5	18	28	42	106	26	4.83	0.91	3.90	0.54	2.92	0.53	1.62	0.23	1.57	0.25	1.41
17PC-79	415.5	32.3	9	8	16	42	63	13	2.45	0.42	1.90	0.25	1.42	0.26	0.81	0.15	0.90	0.15	2.16

17PC-81	425.5	33	3	5	11	33	37	8	1.58	0.23	1.18	0.16	0.79	0.18	0.55	0.10	0.56	0.09	2.00
17PC-82	430.5	33.4	4	7	6	14	20	5	1.04	0.21	1.09	0.18	1.10	0.25	0.85	0.14	1.03	0.16	1.55
17PC-83	435.5	33.7	1	7	10	42	34	8	1.40	0.22	1.24	0.18	0.94	0.23	0.71	0.13	0.83	0.12	2.01
17PC-84	440.5	34.1	12	14	27	57	92	20	3.52	0.64	2.68	0.39	2.33	0.44	1.32	0.24	1.39	0.28	2.31
17PC-85	445.5	34.4	2	4	10	32	34	8	1.41	0.20	1.10	0.14	0.66	0.16	0.44	0.09	0.54	0.08	1.84
17PC-86	450.5	34.8	7	11	7	20	29	7	1.71	0.28	1.63	0.30	1.80	0.44	1.25	0.23	1.49	0.24	1.73
17PC-87	455.5	35.1	8	19	35	79	132	31	5.81	0.97	4.38	0.65	3.46	0.59	1.70	0.26	1.54	0.27	2.53
17PC-88	460.5	35.5	7	26	36	51	142	34	6.44	1.07	5.42	0.76	4.16	0.79	2.39	0.38	2.32	0.34	2.02